DEPARTMENT OF THE INTERIOR
U.S. GEOLOGICAL SURVEY

Spectral analysis of aeromagnetic profiles for depth estimation

principles, software, and practical application

by

H. S. Sadek, S. M. Rashad, and H. R. Blank[1/]

Open-File Report 84- 849

Prepared for the Ministry of Petroleum and Mineral Resources, Deputy Ministry for Mineral Resources, Jiddah, Kingdom of Saudi Arabia

1/ U.S. Geological Survey Mission, Saudi Arabia

1984

CONTENTS

APPENDICES

ILLUSTRATIONS

TABLE

SPECTRAL ANALYSIS OF AEROMAGNETIC PROFILES FOR DEPTH ESTIMATION: PRINCIPLES, SOFTWARE, AND PRECTICAL APPLICATION

by

Hamdy S. Sadek, S.M. Rashad,
and H. Richard Blank

ABSTRACT

Fourier spectral analysis in recent years has become a widely utilized tool for the processing and interpretation of potential field data. It is particularly well suited to analysis of aeromagnetic maps and profiles, where coverage commonly is of broad scope and statistical treatment is appropriate.

The techniques developed by earlier workers for map data are readily adapted for depth estimates using aeromagnetic profiles. Three subroutines are presented: "FRQAN", which employs the complete Fourier transform to convert field intensity to the frequency domain and then computes the logarithmic energy spectrum; "CSIZE", which refines the spectrum to correct for the finite horizontal dimensions of magnetic sources, and "ENSMTH", which smooths the spectrum to clarify its decay characteristics. The average depths to sources of ensembles are obtained by manually fitting a straight line to each linear interval of the logarithmic energy-decay curve.

If proper account is taken of the constraints of the method, it is capable of providing depth estimates to within an accuracy of about 10 percent under suitable circumstances. The estimates are unaffected by source magnetization and are relatively insensitive to assumptions as to source shape or distribution. The validity of the method is demonstrated by analyses of synthetic profiles and profiles recorded over Harrat Rahat, Saudi Arabia, and Diyur, Egypt, where source depths have been proved by drilling.

INTRODUCTION

The computational efficiency and storage capacity of modern digital computers now permit geophysicists to utilize a wide variety of sophisticated mathematical techniques for data processing and analysis. In particular, the method of Fourier spectral analysis has attracted increasing attention in recent years as a tool for the interpretation of potential field data. Whether employed independently or coupled with conventional time domain analysis, the spectral or frequency domain approach commonly results in a significantly more intensive and complete evaluation of aeromagnetic and gravity data than is otherwise attainable. It has proved to be especially useful where data coverage is of broad scope and statistical treatment of field disturbances arising from multiple sources is appropriate. Under such circumstances, determination of the average depth to the causative bodies may be of paramount interest, and it is in statistical depth estimation that the surprisingly simple but elegant techniques of spectral analysis, properly applied, can often be uniquely effective. The purpose of this report is to present a software package for the computation and refinement of Fourier energy spectra of aeromagnetic profiles, and, at the same time, to review the underlying principles of the spectral method and point out some practical constraints on the estimation of depth from the spectra. The method is illustrated by a number of synthetic and real examples.

Background

The idea of using Fourier spectra for the analysis of geophysical potential field data is sometimes attributed to Dean (1958), although he was anticipated by Serson and Hannaford (1957), who used autocorrelation functions to carry out a statistical analysis of aeromagnetic profiles, and possibly by others. Early applications include the works of Alldredge and others (1963) and Horton and others (1964) on statistical analysis of aeromagnetic profiles and maps, respectively. The anomalies and autocorrelation functions associated with simple 2-D (two-dimensional and 3-D (three-dimensional) magnetic and gravity models were subsequently transformed mathematically to the frequency domain by Bhattacharyya (1966), Spector and Bhattacharyya (1966), Spector (1968), Rao and Avasthi (1973), Cassano and Rocca (1975), Bhismasankaram and others (1977), Regan and Hinze (1977, 1978), Chowdary (1978), and Pedersen (1978b). Bhattacharyya (1967) and Pedersen (1978a) also developed expressions for the spectra of generalized source distributions.

In addition to these formulations, considerable progress has been made in the development of methods of inversion of areally extensive blocks of data by frequency analysis. The statistical approach of early workers has been greatly

extended by Spector (1968), Spector and Grant (1970), and Pedersen (1978b), particularly in regard to depth estimation. Successful use of radial Fourier energy spectra of aeromagnetic maps for depth estimation is illustrated in the works of the above authors and elsewhere (for example, Spector and Parker, 1979; Sadek, 1978; Meshref and others, 1980; Sadek and others, 1983). Building on the theoretical developments especially of Bhattacharyya (1967) and Spector (1968), several authors have also shown that operations such as wavelength filtering, trend filtering, differentiation, continuation, and magnetic reduction-to-the-pole can be efficiently carried out in the frequency domain. A general review of systematic computational schemes is given by Spector and Parker (1979).

The statistical methods of map interpretation are readily adapted to profiles. A comprehensive and succinct review of the profile problem has been published by Green (1972). While in some ways not as satisfactory as map analysis and perhaps subject to more pitfalls, the profile technique is nevertheless capable of providing reasonably accurate depth estimates. Recently reported examples include spectral analysis of aeromagnetic profiles over Tertiary volcanics in the Silet region of Algeria (Curtis and Jain, 1975), and over late Cenozoic lavas of Harrat Rahat, Saudi Arabia (Blank and Sadek, 1983). In both of these studies the analysis yielded the thickness of volcanic cover rock on a concealed basement.

Outline of the method

Sequential steps in the spectral method of depth estimation, whether applied to single or multiple anomalies and whether the data are in map or profile form, are as follows: a linear or planar regional field is first removed from the digital image of the field in the space domain, the field is then transformed to the frequency domain, the energy spectrum is calculated from the complex Fourier amplitude spectrum, and the logarithm of the energy is plotted against radial frequency or wave number. If the raw data are in map form, the energy is a function of both radial frequency and radial azimuth direction, and the most appropriate linear plot of energy decay may be an average of the decay in several radial directions, but in the case of single profiles the azimuth is of course just the profile azimuth. An average horizontal source width is obtained, either directly from the data by measurement of distances between points of inflection on anomalies or from their second vertical derivatives, and the spectrum is "refined" accordingly. Finally the average source depth is obtained from the slope of the linear portion of the energy-decay curve. Appreciable changes in the dominant gradient indicate the presence of sources at more than one characteristic depth; each linear interval must be analyzed separately. If the decay curve is completely

nonlinear, an approximate source depth can sometimes be obtained directly from the position of the energy maximum, if well defined, or by linearizing the decay through further refinement.

The algorithm employed in computation of the energy spectrum in our work is similar to that employed by Spector (1968) for map analysis. It is significant that Spector computed the Fourier transform of field data by the method of Filon (in Tranter, 1962), rather than by use of the Fast Fourier Transform (FFT) algorithm of Cooley and Tukey (1965). Filon's method is computationally slower than the FFT but, unlike the latter, does not produce unacceptable distortions at high frequencies (see Cordell and Grauch, 1982). Other advantages of this technique are pointed out in an analysis by Sadek (in press).

As implied above, the shape of the computed spectrum is substantially affected by the finite average horizontal size or width of anomaly sources when the widths are large compared with source depths, and in order to utilize the spectrum for depth estimates it may first be necessary to remove this influence. Algorithms employed in modifying the spectrum to compensate for horizontal size effect are adopted from Spector (1968) and Pedersen (1978b). The spectral computation and refinement algorithms are developed in the text which follows, and the associated computer subroutines are listed in appendices A and B. A subroutine for smoothing the energy spectrum is listed in appendix C.

We have chosen not to automate the depth estimation itself, although a least-squares fit to linear intervals of the energy-decay curve is easily programmed. Also, the initial removal of a first-order regional gradient from the data (to avoid masking of the contribution of deep-seated sources) can readily be carried out by a separate subroutine.

COMPUTATION OF THE ENERGY SPECTRUM

The Fourier integral transform of a function that varies continuously along a profile of observation, such as the gravity or magnetic field intensity, transforms the function from the space to the frequency domain, and is expressed by

$$\Delta\bar{T}(f_y) = \int_{-\infty}^{\infty} \Delta T(y) \cdot e^{-2\pi f_y y} dy \quad , \tag{1}$$

where

$\Delta\bar{T}(f_y)$ = Fourier transform of $\Delta T(y)$,

f_y = spatial frequency in the direction of the y-axis (cycles/unit length),

$\Delta T(y)$ = potential-field intensity along y-axis, and

y = linear distance along the profile.

In order to apply the Fourier transform to a function that is bounded in y, as in the case of a profile of finite length, it must be assumed that the function is periodic outside the given range of y. This effectively collapses the integration range to the interval of the data, since no additional spectral information is contained outside this interval. It is desirable for the data to have zero mean for numerical reasons (to prevent round-off errors due to a very large zero-frequency component). Therefore the data are routinely detrended and brought to zero mean before applying spectral analysis. Physically, this amounts to removing long-wavelength components not defined by the finite data interval.

Also it is desirable for the data to have equal values at the two endpoints; otherwise a discontinuity will be present at the onset of each cyclic repetition. A Fourier series representation of the data at such a discontinuity will always yield the mean value of the bracketing function values even if the number of terms in the series is infinite. The spectrum is thereby distorted and cannot faithfully represent the data in the vicinity of the endpoints. Endpoint discontinuities can be eliminated by multiplying the field intensity by a weighting function that smoothes the intensity to zero at the extremities of the data segment. Since the Fourier transform of this product is the Fourier transform of the field intensity along the segment convolved with the Fourier transform of the weighting function, it is necessary to choose the weighting function so as to minimize distortion introduced in the spectrum by the convolution process. A Hanning "cosine bell" function G(y), centered at the midpoint of the field-intensity segment, introduces negligible spectral distortion when transformed and convolved with the data transform, while suppressing the contribution of field anomalies near the data extremities. This center-weighting is highly advantageous as a means of focusing the analysis. Following Spector (1968) we employ the Hanning window in the present work, and rewrite equation (1)

$$\Delta\bar{T}(f_y) = \int_{-L_y/2}^{L_y/2} \Delta T(y)\cdot G(y)\cdot e^{-i2\pi f_y y}dy \quad , \tag{2}$$

where

L_y = length of profile in the interval - $L_y/2$

and

$$G(y) = 1/2(1+\cos(2\pi y/L_y)) . \tag{3}$$

Defining the wave number v as

$$v = 2\pi f_y \tag{4}$$

and using Euler's theorem

$$e^{-ivy} = \cos(vy) - i\sin(vy) \quad , \tag{5}$$

we get from (2)

$$\Delta\bar{T}(v) = \int_{-L_y/2}^{L_y/2} \Delta T(y)\cdot G(y)\cdot\cos(vy)\,dy - i\int_{-L_y/2}^{L_y/2} \Delta T\cdot G(y)\cdot\sin(vy)\,dy \; . \tag{6}$$

If we define in addition

$$\Delta T_1(y) = \Delta T(y)\cdot G(y) \tag{7}$$

$$I_c = \int_{-L_y/2}^{L_y/2} \Delta T_1(y)\cdot\cos(vy)\,dy \tag{8}$$

$$I_s = \int_{-L_y/2}^{L_y/2} \Delta T_1(y)\cdot\sin(vy)\,dy \quad , \tag{9}$$

then

$$\Delta\bar{T} = I_c - iI_s \quad . \tag{10}$$

Thus the Fourier transform can be evaluated as the complex sum of two trigonometric integrals.

When y is not small, the numerical evaluation of the integrals is a matter of considerable difficulty. Because of the rapid oscillation of the functions cos (vy) and sin (vy), the use of ordinary quadrature formulae such as Simpson's Rule require division of the range of integration into such small steps that the computation is impractically lengthy. However, as recognized by Spector (1968, p. 3.26 ff), a much more efficient numerical solution for the integration of trigonometric functions has been provided by Filon (in Tranter, 1962). Filon's solution is a modification of Simpson's quadrature formula and involves fitting of T in successive intervals of Y_{j-1} , Y_{j+1} with parabolic arcs. By this method, the numerical solution of a cosine integration in the form of equation (8) is given by

$$I_c(v) = \Delta y\left\{(\Delta T_1(N_y) + \Delta T\ (1))\alpha\sin(vL_y) + \beta c_1 + \gamma c_2\right\} \tag{11}$$

where

Δy = data sample increment

N_y = number of data sample points

$L = L_y/2$

$\theta = y\Delta y$

$$\alpha = \theta^{-3}(\theta^2 + \theta\sin\theta\cos\theta - 2\sin^2\theta) \quad (12)$$

$$\beta = 2\theta^{-3}(\theta(1+\cos^2\theta) - 2\sin\theta\cos\theta) \quad (13)$$

$$\gamma = 4\theta^{-3}(\sin\theta - \theta\cos\theta) \quad (14)$$

Similarly, the numerical solution of the sine integration is

$$I_s(v) = \Delta y \left\{ -(\Delta T_1(N_y) - \Delta T_1(1))\alpha\cos(vL_y) + \beta s_1 + \gamma s_2 \right\} . \quad (15)$$

If we let

$$N_c = (N_y - 3)/2 \quad (16)$$

$$N_s = (N_y - 1)/2 \quad (17)$$

then the integration constants C1, S1, C2, S2 are given by

$$C1 = \sum_{j=1}^{N_c} \Delta T_1(2j+1)\cos(v(2j\Delta y - L_y)) + 1/2(\Delta T_1(N_y) + \Delta T(1))\cos(vL_y) \quad (18)$$

$$C2 = \sum_{j=1}^{N_c} \Delta T_1(2j)\cos(v(2j-1)\Delta y - L_y) \quad (19)$$

$$S1 = \sum_{j=1}^{N_s} \Delta T_1(2j+1)\sin(v(2j\Delta y - L_y)) + 1/2(\Delta T_1(N_y) - \Delta T(1))\sin(vL_y) \quad (20)$$

$$S2 = \sum_{j=1}^{N_s} \Delta T_1(2j)\sin(v(2j-1)\Delta y - L_y) \quad (21)$$

Note that if y and therefore $\theta = 0$, then

$$\alpha = 0 \ , \ \beta = 2/3 \ , \ \gamma = 4/3$$

and

$$I_c = \Delta y/3\left(2\sum_{j=1}^{N_c} \Delta T_1(2j+1) + 4\sum_{j=1}^{N_s} \Delta T_1(2j) + \Delta T_1(N_y) + \Delta T_1(1)\right) , \quad (22)$$

which is Simpson's Rule. Substituting the expressions for the cosine and sine integrations (I_c, I_s) in equations (11) and (15) in equation (10), we get a numerical solution of the integral Fourier transform. This algorithm is

employed in subroutine "FRQAN" (appendix A), which computes the energy spectrum.

The Fourier transform $\Delta\bar{T}(f_y)$ is expressed in terms of negative as well as positive frequencies, but since the transform is a symmetric function about $f_y = 0$, the energy corresponding to f_y is the same as that corresponding to $-f_y$ and only positive frequencies need be employed.

The energy density function $E(f_y)$ is obtained through multiplication of the Fourier transform by its complex conjugate $\Delta\bar{T}^*(f_y)$:

$$E(f_y) = \Delta\bar{T}(f_y) \cdot \Delta T^*(f_y) \quad . \tag{24}$$

Finally, the natural Napierian logarithmic values of $E(f_y)$ are plotted against frequency to produce a logarithmic energy spectrum, or spectral energy-decay curve.

Figure 1 illustrates the input/output parameters involved in the Fourier transformation from the space to the frequency domain. The plotting interval, Δf_y , is determined by the smoothing characteristics of the Hanning window, which impose a practical limit to the attainable frequency resolution. This limit in the space domain is just the fundamental harmonic of the profile (one cycle in the total length L_y). All other frequencies plotted are then multiples of Δf_y , or higher harmonics; no additional information is obtained by plotting at a finer interval. The upper limit on the frequency plot is generally set at the Nyquist (folding) frequency, which is determined by the initial data sample interval. Thus the logarithmic energy is plotted at

$$f_j = j\Delta f_y = j/L_y \quad , \quad j = 0,1,2,\ldots,n \quad .$$

$f_o = 0$, the D.C. level

$f_1 = 1/L_y$, the frequency interval

$f_n = n\Delta f_y = 1/2\Delta y$, the Nyquist frequency,

it follows that the number of points plotted is

$$\begin{aligned} N_f &= n+1 \\ &= (1/2\Delta y / 1/L_y)+1 \\ &= ((N_{y-1})/2)+1 \end{aligned} \tag{24a}$$

where the number of data sample points N_y is given by

$$N_y = L_y/\Delta y+1 \quad , \tag{25}$$

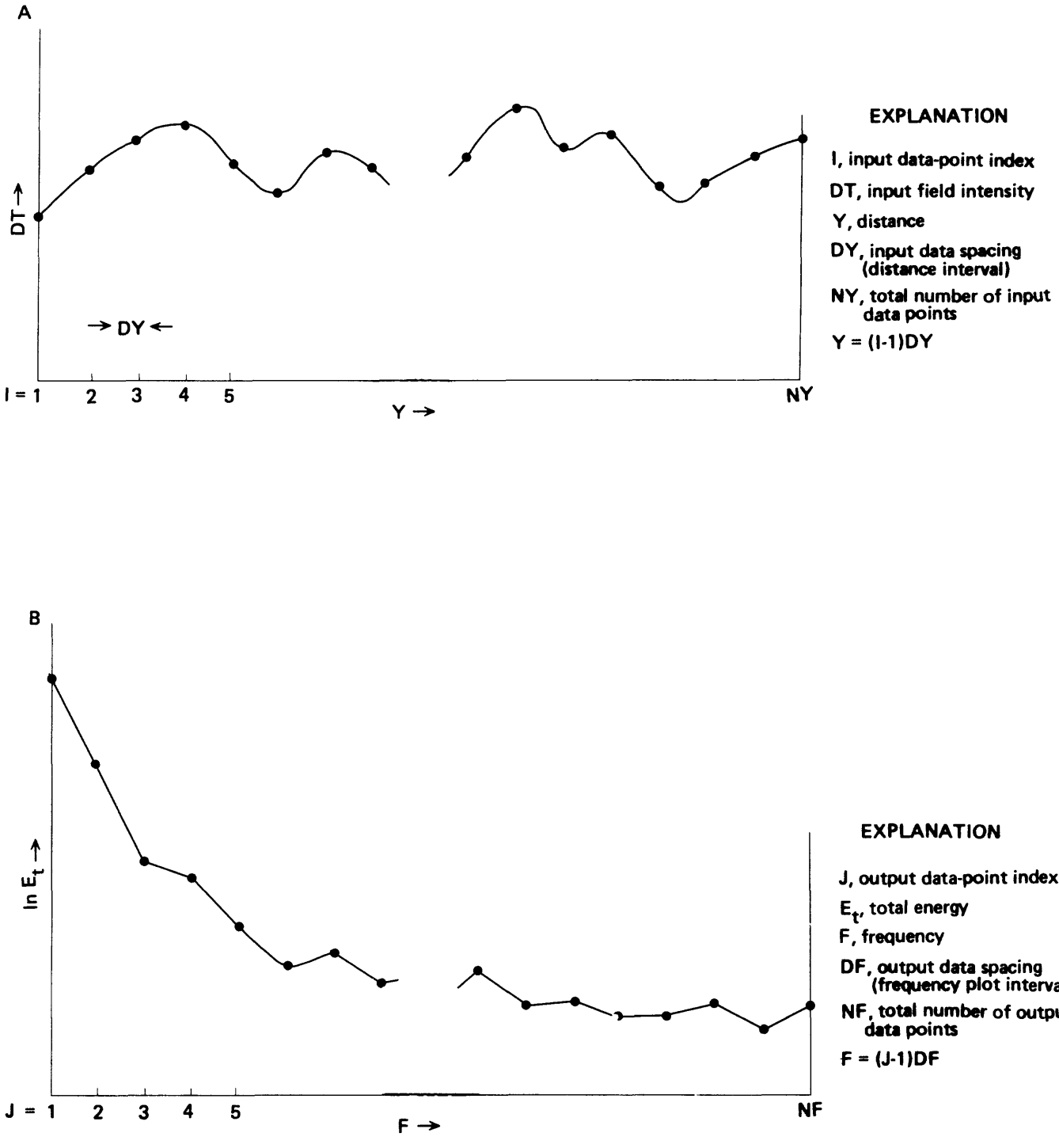

Figure 1.--Input-output parameters, numerical Fourier transformation. A, Space Domain (input), B, frequency domain (output).

The spectrum will in fact contain energy at frequencies greater than the Nyquist frequency, but if the field data sample interval is sufficiently fine, that is, if there are no "spikes" in the sampled field intensity (which in practice requires that the sample interval be no greater than about one-quarter of the width of the sharpest anomalies present), then these frequencies represent only white noise due to round off errors, and the corresponding energy is reflected uniformly back through the spectrum. Aliasing, as the reflection phenomenon is known, can be minimized by preliminary application of a suitable high-cut filter to the data (before weighting), as for example when the data digitization interval is finer than the interval desired for frequency analysis, or when the continuous field contains significant variations within horizontal distances that are short relative to the digitization interval.

The distortion of the spectrum as a result of convolution with a spectral window (Hanning function) also determines the maximum depth of investigation of anomaly sources. For the distortion to be tolerable, the maximum depth cannot exceed about a quarter of the wavelength of the fundamental harmonic, that is, about $L_{y/4}$. In practice, the maximum depth may be much less than $L_{y/4}$, particularly when the spectrum decays rapidly in relation to the energy level of noise introduced by round-off error in the recorded data. The corresponding limit in map analysis is about one quarter of the minimum map width (Spector, 1968).

When the data are in the form of long profiles, the analysis is sometimes best carried out using discrete segments of each profile, in order to improve the horizontal resolution of estimated depth variations and also to minimize the effects of source-depth dispersion. Selection of an optimum segment length is largely empirical, but must take into account the depth of investigation desired and the difficulty in characterizing a spectrum that decays very rapidly or has a low signal-to-noise ratio. An example of the effect of varying the segment length is given by Blank and Sadek (1983).

CHARACTERISTICS OF THE ENERGY SPECTRUM

General form of the energy equation for simple source configurations

We next examine the characteristics of the spectrum for ideal source configurations, and the way in which these characteristics are exploited in depth estimations. An important feature of the spectrum for many simple source shapes (points, lines, and flat-topped bodies) is that it can

be expressed as the product of discrete factors, viz.

$$E(r,\theta)=M\cdot R_M(\theta)\cdot R_T(\theta)\cdot H(h,r)\cdot S(a_i,r,\theta)\cdot C(b_i,r) \qquad (26)$$

where

M = scalar-magnetization factor, involving only the magnitude of the body magnetization

R_T = geomagnetic field factor, involving only the direction cosines of the earth's field

R_M = vector-magnetization factor, involving only the direction cosines of the source magnetization (assumed to be uniform)

H = depth factor

S = horizontal size (width) factor

C = vertical size (thickness or depth extent) factor;

and

r = radial wave number ($r = 2\pi f$, where frequency f can be measured in any direction in the x-y plane)

θ = azimuth of the radial wave number

h = depth to the top of the model source

a_i = parameters related to the horizontal dimensions of the source

b_i = parameters related to the the vertical depth extent of the source

These factors are combined in various ways by different authors.

From equation (26), we see that only the factors H, S, and C affect the radial spectrum; the factors M, R_M, and R_T affect only the absolute value of the energy and its change with respect to azimuth, and in no way affect the shape of the energy-decay curve plotted as a function of wave number or frequency. Moreover, when the logarithm of energy is plotted the factors become additive.

The decay of spectral energy with increasing frequency is almost invariably dominated by the depth factor, which for

all simple source geometries is given by

$$H(h,r) = e^{-2hr} \qquad (27)$$

Thus, for single models, a rough estimate of depth to the top can be obtained by measuring the slope of the logarithmic energy decay. The accuracy of this first estimate depends on the extent to which the factors S and C affect the spectrum.

The S- and C-factors for a number of simple 3-D and 2-D models are shown in table 1. Expressions given for prismatic sources assume sides parallel to the reference axes, and for 2-D bodies the profile is assumed to be normal to the strike and in the x direction. For a point source (pole or dipole) and for a 2-D point source (line of poles or dipoles) or thin infinite dike (half sheet), the horizontal size factor is unity. It is also unity for the spectrum of the gradient of a semi-infinite horizontal slab normal to the strike of the interface, as pointed out by Cassano and Rocca (1975). The vertical size (depth extent) factor is unity only for point poles or horizontal lines of poles, and for models which are not "depth limited," that is, for infinite vertical circular cylinders, vertical prisms, or vertical dikes. The C-factor for infinite thin inclined dikes is a function only of the dike inclination. For all other source configurations shown on table 1 it is clear that the factors S and C can both have a significant effect on the radial spectrum.

Two relatively simple depth-limited models are the point dipole and the small horizontal lamina. In each case the size effect is nil or negligible, and the C-factor results in a spectral maximum at a wave number $r = 1/h$. For bottomed vertical prisms, bottomed cylinders, or bottomed dikes of vertical depth extent t, the C-factor gives rise to a spectral maximum at

$$r = 1/t \cdot \ln((h+t)/h) \quad , \qquad (28)$$

provided the effect of the horizontal size factor is negligible or has been compensated. The bottomed cases are very close to the laminar case at $t/h \leqslant 0.25$ and to the bottomless case at $t/h \geqslant 1.0$; for intermediate values of t/h, the energy decays linearly only at high frequencies.

Expectation of the energy for source ensembles

The ideal case of an anomaly due only to a single, simple source body does not very often occur in nature, and we are therefore interested in the form of the spectrum in the more general case when field distrubances along a profile are due to multiple sources. Spector (1968) apparently first introduced the concept of source ensembles. He evaluated the

Table 1.--Size factors in general energy equation for simple models

Explanation: r = radial wave no. = $2\pi(f_x^2+f_y^2)^{1/2}$; f_x, f_y = frequencies in x,y directions; $u = r\sin\theta = 2\pi f_x$; $v = r\cos\theta = 2\pi f_y$; $\theta = \tan^{-1}(u/v)$

a = half length of line, radius of cylinder, or horizontal half width of dike; a,b = half widths of prism or lamina in x,y directions; ψ = angle made by line with x-axis; Φ = dip of dike, t = vertical depth extent (extent in z-direction)

J_1 = first-order Bessel Function

Model	Factor S (a, b, ψ, r, θ) Horizontal size	Factor C (t, Φ, r, θ) Vertical size	Reference
3-D Models:			
point pole	1	1	Spector (1968)
point dipole	1	r^2	Spector (1968)
finite horizontal line of poles	$\frac{\sin^2[a(u\cos\psi + v\sin\psi)]}{a^2(u\cos\psi + v\sin\psi)^2}$	1	Spector (1968)
finite horizontal line of dipoles	$\frac{\sin^2[a(u\cos\psi + v\sin\psi)]}{a^2(u\cos\psi + v\sin\psi)^2}$	r^2	Spector (1968)
infinite vertical rectangular prism	$\frac{\sin^2(au)}{(au)^2}\ \frac{\sin^2(bv)}{(bv)^2}$	1	Spector (1968)
finite vertical rectangular prism	$\frac{\sin^2(au)}{(au)^2}\ \frac{\sin^2(bv)}{(bv)^2}$	$(1-e^{-tr})^2$	Spector (1968)
horizontal rectangular lamina	$\frac{\sin^2(au)}{(au)^2}\ \frac{\sin^2(bv)}{(bv)^2}$	$(tr)^2$	Pedersen (1978b)
infinite vertical circular cylinder	$\frac{J_1^2(ar)}{(ar)^2}$	1	Pedersen (1978b)
finite vertical circular cylinder	$\frac{J_1^2(ar)}{(ar)^2}$	$(1-e^{-tr})^2$	Pedersen (1978b)
2-D Models:			
horizontal line of poles	1	1	
horizontal line of dipoles	1	u^2	
infinite thin inclined dike; gradient of horizontal slab with inclined face	1	$\sin^2$	Cassano/Rocca (1975)
infinite vertical dike	$\frac{\sin^2(au)}{(au)^2}$	1	Pedersen (1978b)
finite vertical dike	$\frac{\sin^2(au)}{(au)^2}$	$(1-e^{-tu})^2$	Pedersen (1978b)
finite inclined dike	$\frac{\sin^2(au)}{(au)^2}$	$\sin^2\ [1+e^{-2tu}-2e^{-tu}\cos(\cot\Phi\ tu)]$	Pedersen (1978b)

expectation (most probable value) of the energy spectrum of an ensemble on the assumption that the expectation is the ensemble average value. This may be expressed as

$$\langle E(r,\theta)\rangle = \int_V E(r,\theta)\cdot\Phi(P_i)\,dV, \quad i=1,2,\ldots,n, \tag{29}$$

where

V = n-parameter space

Φ = joint probability distribution function for parameters P_i.

On the further assumption that the parameters vary independently of one another, we may write

$$\Phi(P_i) = \Phi(P_1)\cdot\Phi(P_2)\ldots\ldots\Phi(P_n) , \tag{30}$$

and hence, analogous to equation (26),

$$\langle E(r,\theta)\rangle = \langle M\rangle\langle R_M(\theta)\rangle\langle R_T(\theta)\rangle\langle H(h,r)\rangle\langle S(a_i,r,\theta)\rangle\langle C(b_i,r)\rangle \tag{31}$$

For depth estimation our concern is chiefly with the last three factors, $\langle H(r,\theta)\rangle$, $\langle S(a_i,r,\theta)\rangle$, and $\langle C(b_i,r)\rangle$, as previously. The effect of these factors is illustrated schematically in figure 2. We shall now treat each factor in detail.

Depth factor and depth estimation

Following Pedersen (1978b), we consider a source ensemble with a uniform (random) depth distribution such that

$$h(1-\gamma) \leq h \leq \bar{h}(1+\gamma) , \tag{32}$$

where $\gamma \leqslant 1$ and $\bar{h}$ = average value of h. The sources can be any of the types listed in table 1. Then

$$\langle H(h,r)\rangle = \frac{1}{2\gamma\bar{h}} \int_{h(1-\gamma)}^{\bar{h}(1+\gamma)} e^{-2hr}\,dh \tag{33}$$

Pedersen evaluated this integral and plotted $\partial \ln\langle H\rangle/\partial hr$, showing that the slope is asymptotic to $2(1-\gamma)$ for any γ, for example, when

$\gamma = 0$, slope = 2: all depths are the same and are obtained directly from the plot of $\ln \langle H \rangle$ vs. r

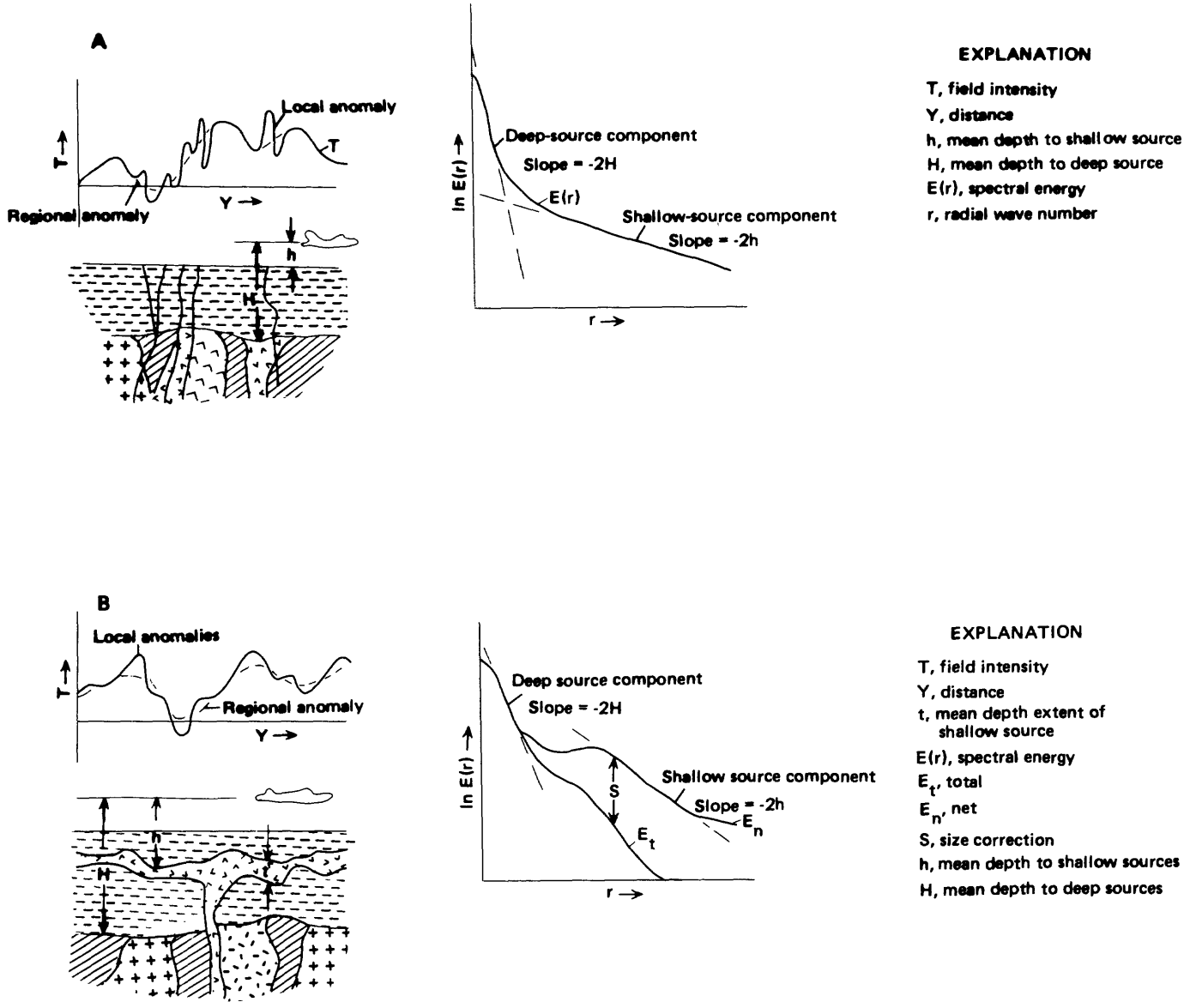

Figure 2.- Factors showing effect of source depth, width, and depth extent on logarithmic spectral energy-decay curve. A, Shallow and deep sources, both with very great depth extent but limited width. A linear segment of the decay curve is associated with each source ensemble. B, Shallow sources of limited depth extent but appreciable width; deep sources as in A. A width ("size") correction flattens the slope of the decay curve and is especially significant at large wave numbers. Note the broad energy maximum resulting from limited depth extent.

γ = 0.5, slope = 2 only at r=0 and is asymptotic to 1.0 for large r, so that a serious underestimation of depth occurs if high frequencies are used in the slope measurement.

The problem was initially addressed by Spector (1968), who concluded that the depth estimate is satisfactory provided the depth variation h is such that

$$\Delta h/h \leqslant 25\% \tag{34}$$

which corresponds to $\gamma = 0.25$. But it is still necessary to avoid large values of $\bar{h}r$ in making the slope measurement, and above all to consider the effects of the horizontal-size and depth-extent factors.

When the spectrum has been refined to correct for the finite horizontal size and limited depth extent of sources, where such corrections are appropriate (see below), then the average depth measured is simply

$$\bar{h} = -\frac{\text{slope}}{4\pi} \tag{35}$$

when the slope is measured on a plot of ln $E(f, \theta)$ vs. f, or

$$\bar{h} = -\frac{\text{slope}}{2} \tag{36}$$

on a plot of amplitude spectrum ln $A(f,\theta)$ vs f. If two or more source ensembles are present, each with a characteristic average source depth and $\Delta h/h \leqslant 25$ percent, then the plot will show a corresponding number of linear intervals and the depths can be determined by measuring the slope of each interval separately, as noted earlier.

Horizontal size (width) factor: refinement of the spectrum

This factor is model dependent and is generally important if the average horizontal dimensions of sources in an ensemble are equal to or greater than the average depth. For any horizontal size (width) of source, the magnitude of the S-factor increases as the frequency increases, but the magnitude changes most rapidly at low frequencies. In all cases the effect is to cause a more rapid decay of the energy with frequency, which results in an overestimation of the

depth unless compensated. Note that the sign of this effect is exactly opposite to that of the depth-dispersal effect. To some extent, therefore, the two effects counterbalance one another. However, the horizontal size effect is generally much larger, and without refinement of the spectrum for this effect the estimated depths must be regarded as maximum values.

In order to evaluate the size effect, we refer first to Pedersen (1978b). Assume that the sources are vertical circular cylinders of radius a, with uniform distribution such that

$$0 \leqslant a \leqslant 2\bar{a} \quad , \tag{37}$$

where $\bar{a}$ = average radius. Then from table 1, the expectation of the S-factor is

$$\langle S \rangle = \frac{1}{2\bar{a}} \int_0^{2\bar{a}} \frac{J_1(ar)^2}{ar}\, da \tag{38}$$

$$= \frac{8}{3\pi \bar{a} r} \quad , \quad \bar{a}r > \pi \tag{39}$$

, that is, in the asymptotic range for evaluation of the integral. Thus the rate of energy decay due to S is given by

$$\frac{\partial \ln \langle S \rangle}{\partial r} = -\frac{1}{r} \quad , \tag{40}$$

compared with the rate due to H.

$$\frac{\partial}{\partial r} \ln \langle H \rangle = -2\bar{h} \tag{41}$$

For a more restrictive size distribution, viz.

$$\bar{a}(1-\beta) \leqslant a \leqslant \bar{a}(1+\beta) \quad , \beta < 1 \quad , \tag{42}$$

the rate of decay due to the S factor for the cylindrical model turns out to be

$$\frac{\partial \ln \langle S \rangle}{\partial r} = -\frac{3}{r} \quad , \quad \bar{a}r > \pi \tag{43}$$

In other words, the effect is three times as large as for $\beta = 1$.

It was shown by Pedersen (1978b) that for a dike model with average horizontal half width $\bar{a}$, the result at $\beta = 1$ is the same as for the cylinder, but that when $\beta = 1$ the rate of decay is

$$\frac{\partial}{\partial r} \ln \langle S \rangle = -\frac{2}{r} , \quad \bar{a}r > \pi , \tag{44}$$

or two rather than three times the rate of decay with $\beta = 1$. Finally, Pedersen considers the vertical prism model, with half widths a and b uniformly distributed such that

$$\bar{a}(1-\beta) \leqslant a \leqslant \bar{a}(1+\beta) \tag{45}$$

$$\bar{a}(1-\beta) \leqslant b \leqslant \bar{a}(1+\beta) , \quad 0 \leqslant \alpha \leqslant 1 , \quad 0 \leqslant \beta \leqslant 1 . \tag{46}$$

The parameter is thus an elongation factor. The expectation of S is obtained by averaging over both of the size parameters and over . The result is that for $\beta = 1$ and various , the asymptotic rate of decay is given by

$$\frac{\partial}{\partial r} \ln \langle S \rangle = -\frac{2}{r} .$$

It is similar to that of the dike with the more restrictive distribution function (equation 44), $\beta < 1$, and twice that of the cylinder (equation 40). For $\beta < 1$, $\alpha < 1$, however, the asymptotic rate is

$$\frac{\partial}{\partial r} \ln \langle S \rangle = -\frac{3}{r} , \tag{47}$$

the same as for the cylinder.

The analysis of Spector (1968) for the case of an ensemble of vertical prisms assumes $\alpha = \beta = 1$, but allows a simple numerical evaluation of the expectation in the lower end of the frequency or wave-number range. Again averaging over 0 and the parameters $\bar{a}=\bar{b}$, we have

$$S(r) = \frac{1}{\pi} \int_0^{\pi} \left\{ \frac{S_i(2\bar{a}r \sin\theta)}{2\bar{a}r \sin\theta} \cdot \frac{S_i(2\bar{a}r \cos\theta)}{2\bar{a}r \cos\theta} \right\}^2 d\theta . \tag{48}$$

Here S_i is the "sine integral", defined as

$$S_i(x) = \int_0^x \frac{\sin P}{P} dp , \tag{49}$$

which can be evaluated numerically from the infinite series

$$S_i(x) = \sum_{n=0}^{\infty} \frac{(-1)^n \cdot x^{2n+1}}{(2n+1)\,(2n+1)!} \quad . \tag{50}$$

For computation of the size effect in this work we have elected to employ equation (48) to compute the effect at wave numbers given by $\bar{a}r < \pi$, and to employ Pedersen's asymptotic approximation

$$\langle S(r,\theta) \rangle = \frac{1}{r^2} \tag{51}$$

for $\bar{a}r \geq \pi$. The average width $2\bar{a}$ is obtained by measuring the distance between points of inflection on the profile, or if a map of the data is available, by averaging this distance in orthogonal directions to minimize the possibility of directional bias. Alternatively, it can be obtained from the second vertical derivative of the profile (Green, 1972). Subroutine "CSIZE" (appendix B) has been designed to carry out this computation at frequencies used in subroutine "FRQAN". The subroutine allows the user to refine the spectrum if significant distortions are expected as a result of the finite horizontal size of anomaly sources. The corrections increase with frequency and always result in an increase in energy values, and hence in a decrease in slope and in estimated depths.

When the computation applies to a profile, it is only necessary to carry out the numerical integration for the sine integral once in equation (48), and we delete the integration over level . This procedure stems from an assumption of bidimensionality of sources and choice of one reference axis as the profile direction, so that the wave number in the strike direction is zero (say, $u = r \sin\theta \equiv 0$), and by l'Hospital's Rule

$$\lim_{u \to 0} \left[\frac{\sin 2\bar{a}u}{2\bar{a}u} \right] = 1 \quad . \tag{52}$$

Alternatively, if sources are 3-D rather than 2-D, it is necessary to assume that the integral in equation (48) is independent of θ , so that evaluation at $\theta = 0$ suffices.

We note that for large wave numbers and uniform distribution $0 \leq a \leq 2\bar{a}$, the energy decay for the cylinder and dike (2-D prism) are identical, provided the strike of the dike is normal to the profile, while for the 3-D prism the size effect is similar to that of the cylinder for some size distributions and to that of the dike for others.

The choice of models and size-distribution function for computation of the size correction may seem somewhat arbitrary; indeed, we have used different models for the low-frequency and high-frequency ends of the spectrum (Spector's prism analysis assumes $\alpha = \beta = 1$; that is, that there is no systematic elongation, and leads to an asymptotic effect ($\langle S \rangle = 1/r^3$, not $1/r^2$). Fortunately, the energy-decay rate is not highly sensitive to these choices, nor to the absolute value of the average horizontal size. Yet without any size corrections the depths may be overestimated by as much as 50 to 60 percent or more, especially for deep ensembles that affect most strongly the low frequencies. The only ensemble for which the size effect can be safely ignored is one with source widths corresponding to the shallow limit of resolution of the survey.

One additional effect of the size factor merits comment: the introduction of oscillations in the radial spectrum due to the presence of sine and cosine terms in this factor (see table 1). Such oscillations may tend to be smoothed out in the spectra of dispersed sources or ensembles, but the effect can be readily discerned in spectra of single sources and well-behaved source distributions. In some cases the spacing between minima is quite regular and can be used to determine the source width or average width. Details of this procedure are provided by Spector (1968).

Vertical size (depth extent or thickness) factor

We have already considered the simplest of the depth-limited models (point dipole, line of dipoles, horizontal rectangular lamina) and seen that each produces a logarithmic spectral maximum at $r=1/h$; the linearity of the decay can be restored in this case by subtraction of the term $\ln r^2$ from the spectrum. Similarly, bottomed cylinders, prisms, and dikes produce maxima at a wave number whose value is a function of both depth and depth extent (and in the case of an inclined dike, of the dip). Pedersen (1978b) has closely examined the expectation of the C-factor for the case of ensembles of vertical cylinders, prisms, and dikes (all of which have the same C-factor), with depth extent uniformly distributed such that

$$\bar{t}\,(1-\delta) \leq t \leq \bar{t}(1+\delta) \quad , \quad \delta < 1 \quad . \tag{53}$$

Thus:

$$\langle C \rangle = \frac{1}{2\,\delta\,\bar{t}} \int_{\bar{t}(1-\delta)}^{\bar{t}(1+\delta)} (1-e^{-tr})^2 dt \tag{54}$$

By setting

$$\frac{\partial}{\partial r}\left\{\ln\langle H(r,\bar{h})\rangle+\ln\langle C(r,\bar{t},\delta)\rangle\right\} = 0 \qquad (55)$$

he found a relation between the value of r at the logarithmic energy maximum, which is obtained by inspection of the spectrum, and $\bar{h}$, δ, $\bar{t}$. When $\bar{t}$ is very small this parameter is nearly independent of the distribution parameter but very strongly dependent on δ. When larger, it is strongly dependent on $\bar{h}$. This interdependence makes it very difficult to determine the average depth from the spectrum of depth-limited bodies that are not points or laminae, or to determine the depth extent itself. Spector and Grant (1970) reach the same conclusion by analyzing the situation with $\delta=1$, and essentially dismiss the general depth-limited case as intractable.

Other influences on the spectrum

In addition to the three factors H, S, and C that directly affect the rate of decay of spectral energy as a function of radial frequency, other factors can indirectly influence the shape of the decay curve, particularly when multiple sources are involved. For example, large variations in magnitude and orientation of the source magnetization vector, if systematically dependent on source depth (as may occur for a double ensemble), can affect the depth estimates in the following way. Although neither M nor $R_M(\theta)$ is a function of r in the energy equation (equation 31), each contributes to the absolute level of the energy. Therefore, when ensembles at different depths are characterized by different M and $R_M(\theta)$, the region of the logarithmic decay curve dominated by each will have a different absolute level. This condition may result in a discontinuity or "step" between increments in reality dominated by linear decay. It is conceivable that in some cases the step will be interpreted as a broad maximum, or more likely, that it will obscure the linearity and render the depth estimates less accurate. Spector (1968) and Green (1972) have computed the expectations of M, $R_M(\theta)$, and $R_T(\theta)$ and shown that variations in the orientation of both the magnetization and the earth's field have a negligible effect on the energy spectrum, provided the variations are within about 20° of the average values.

Dispersion of sources in the horizontal plane may strongly affect the azimuthal symmetry of the spectrum and its overall shape in any radial direction. For map analysis, the effect of a nonrandom horizontal source distribution can be minimized by averaging the spectrum over θ. In the case of a single profile it should be borne in mind that the shape

of the energy decay curve is sensitive to the horizontal disposition of anomaly sources relative to the center of analysis, because of the focusing effect of the Hanning weighting function. Anomalies nearest the midpoint of the profile segment yield the maximum spectral energy and hence lend themselves most readily to depth estimation.

Some spectra show a completely nonlinear decay, and no depth estimates can be made. This situation obtains when the source distribution is nearly uniform with depth. In our experience the surface of the uppermost magnetic basement, whatever its nature and however the sources are distributed within that basement, is almost always represented in the energy spectrum as a linear decay interval. However, we concur with the observation of Spector (1968) that the most commonly encountered case is the double ensemble.

Smoothing function

The computed logarithmic energy generally reveals a slowly decreasing mean value within an envelope of erratic rapid variations. The fluctuations in part arise from high-frequency noise reflected back through the spectrum, but they may also express the finite horizontal size effect of sources. If the fluctuations are regularly spaced it may even be possible to deduce the average source width, as we have noted. On the other hand it is sometimes advantageous to smooth the spectrum (suppress the energy scatter) in order to enhance the linearity of the decay for depth estimation. Subroutine "ENSMTH" (appendix C) has been developed to perform this operation by means of a 7-point moving average ("triangular" filter with weighting factors of 1/16, 2/16, 3/16, 4/16, 3/16, 2/16, 1/16). At both ends of the energy decay profile, where the width of the filter window exceeds the number of data points available, the program filters weighted energy values only. As we are concerned only with depth estimation there is no need to compensate for the reduction of energy magnitude by the filtering process (see Green, 1972). The subroutine can be applied to the spectrum either before or after refinement for the size effect.

EXAMPLES OF DEPTH ESTIMATION

Simple magnetic model

A simple magnetic model is the first of three cases chosen to illustrate the application of the spectral method to synthetic data. The anomaly source is represented by an inductively magnetized, bottomless 2-D prism of width 3 km located at a depth of 1.5 km; the length of the body is assumed to be infinite in the magnetic east-west (strike) direction, normal to the profile (fig. 3A). The magnetic

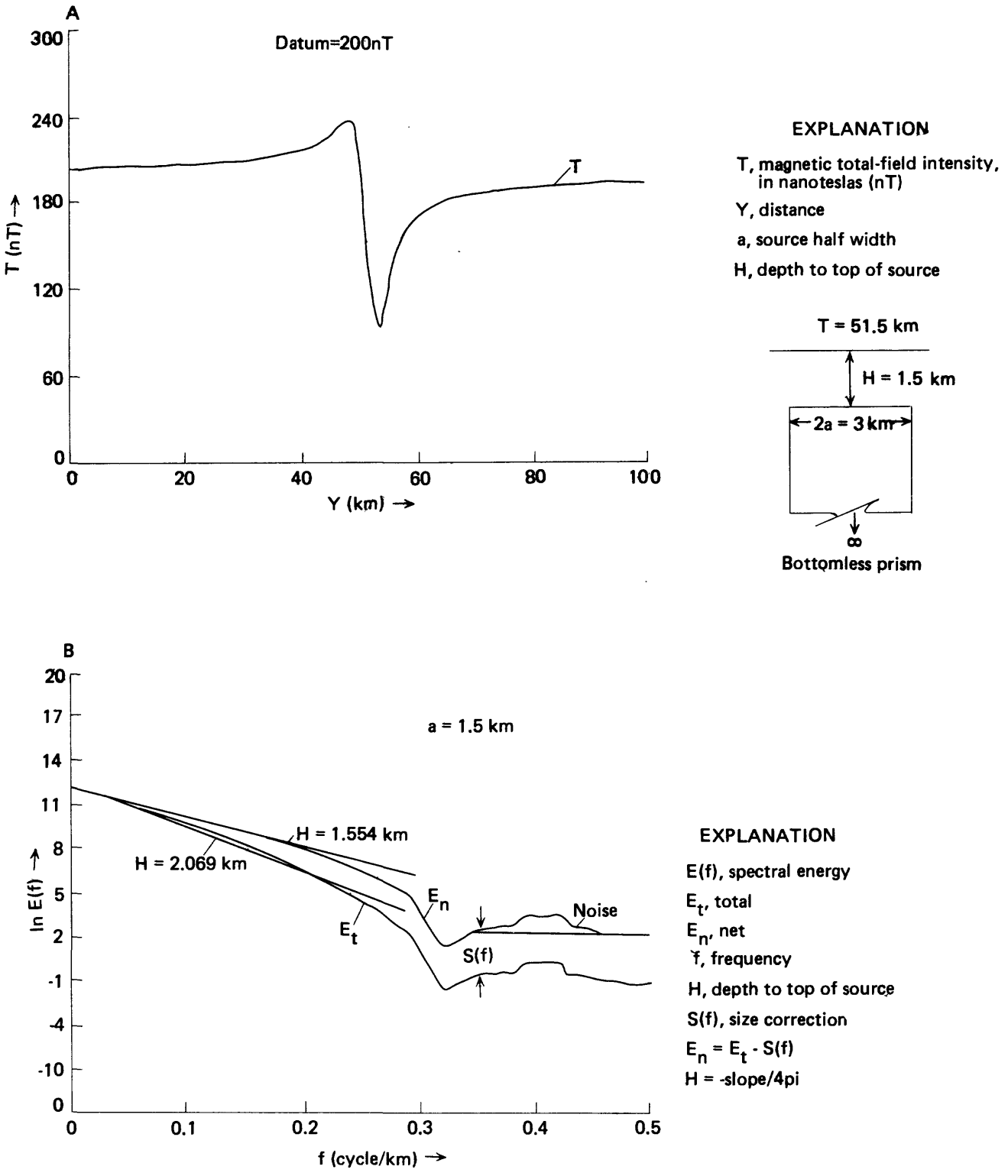

Figure 3.--Spectral analysis of anomaly produced by simple 2-D magnetic test model. A, Space domain. B, Frequency domain. In this and two following figures, anomalous total field intensity was computed using intensity of magnetization 4.2×10^{-3} emu/cm^3 in direction of earth's total field, inclination 30° down.

total field intensity anomaly T was generated using an intensity of magnetization 4.2 X 10^{-3} emu/cm^3 and geomagnetic field inclination 30° down. The profile was then subjected to spectral analysis using subroutine "FRQAN". The resulting logarithmic decay curve is shown in fig. 3B. Examination of the total logarithmic energy curve (E_t) shows that the energy contribution of the model is mainly in the frequency range 0.01 to 0.25 cycle/km. The slope of a line manually fitted to this part of the curve was used to determine the depth to the top of the causative body. A value of 2.07 km was obtained - about 37 percent greater than the actual depth. This overestimation is attributed to the finite horizontal size or width effect in the energy computation. Next, subroutine "CSIZE" was applied, assuming an anomaly half width of 1.5 km, and the net logarithmic energy curve, E_n, was produced. The slope of a line fitted to this new curve in the same frequency interval gives a computed depth of 1.54 km, which is very close to the actual value. Comparison of the two decay curves E_t and E_n shows that the linearity of the decay curve is considerably improved by removal of the size effect.

In figure 4, depth estimates are made from the energy spectrum of a 3-D prismatic model of two orthogonal cross sections identical to that of the 2-D model used in figure 3. The 3-D model (4A) measures 3 X 3 km in the horizontal plane and the total-intensity profile was computed along a median line 1.5 km above the top of the prism, as previously. The total-energy spectral decay curve (E_t) gives an estimated depth of 2.06 km, while the size-corrected curve (E_n) yields a depth of 1.47 km. Thus the result (4B) is essentially the same whether the prismatic source is two dimensional or three dimensional. This observation supports our previous contention that there is no requirement to assume bidimensionality of sources in profile analysis.

Complex magnetic model

In this example (fig. 5A), the source model is an ensemble of three bottomless prisms of widths 3, 4, and 3 km located at depths of 3, 2.5, and 2.7 km, respectively. The total-intensity anomaly was computed using the same earth's field parameters as previously. Spectral analysis was again applied and the corrected and uncorrected logarithmic decay curves of the energy spectrum are shown in figure 5B. The energy contribution of the model ensemble appears in the frequency range 0.05 to 0.4 cycle/km. The slope of a line fitted to the E_t curve in this range gives a calculated average ensemble depth of 3.31 km, which is an overestimation of about 21 percent, as the real average value is 2.73 km. The E_n curve (based on the average model half width of 1.67 km) gives a calculated average depth of 2.69 km, or very close to the actual value.

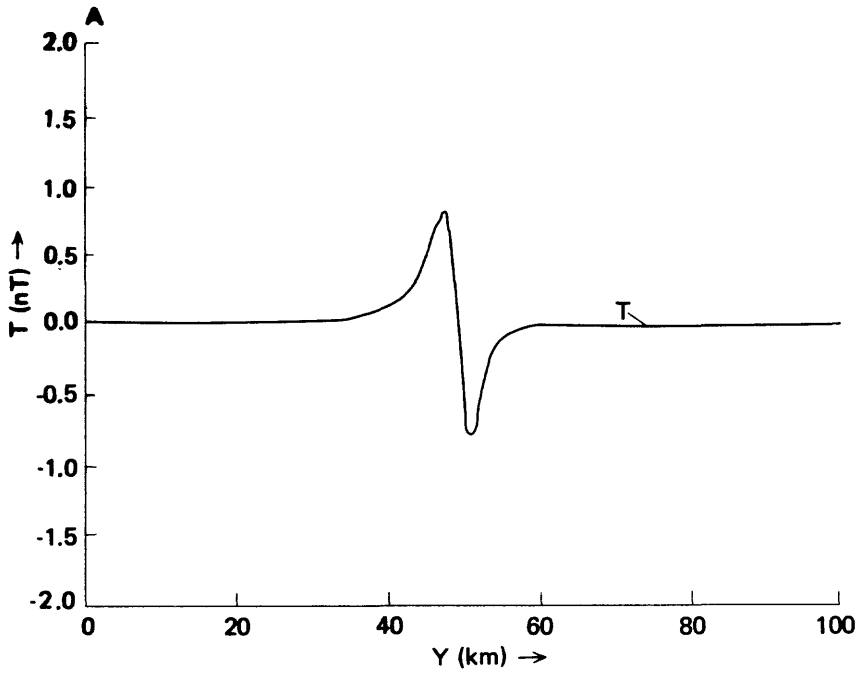

EXPLANATION

T, magnetic total-field intensity, in nanoteslas (nT)

Y, distance

a, source half width

H, depth to top of source

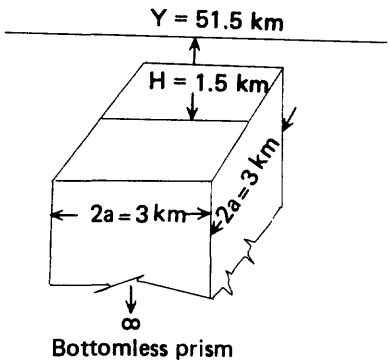

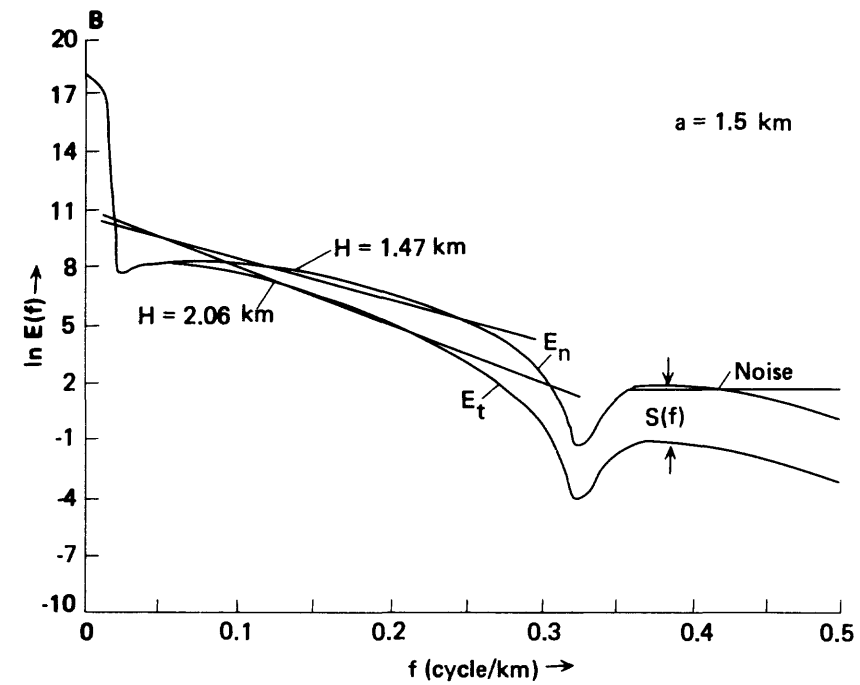

EXPLANATION

E(f), spectral energy

E_t, spectral energy

E_t, total

E_n, net

f, frequency

H depth to top of source

S(f), size correction

$E_n = E_t - S(f)$

H = -slope/4 pi

Figure 4.--Spectral analysis of anomaly produced by simple 3-D magnetic test model of cross section identical to that of model of figure 3. A, Space domain. B, Frequency domain.

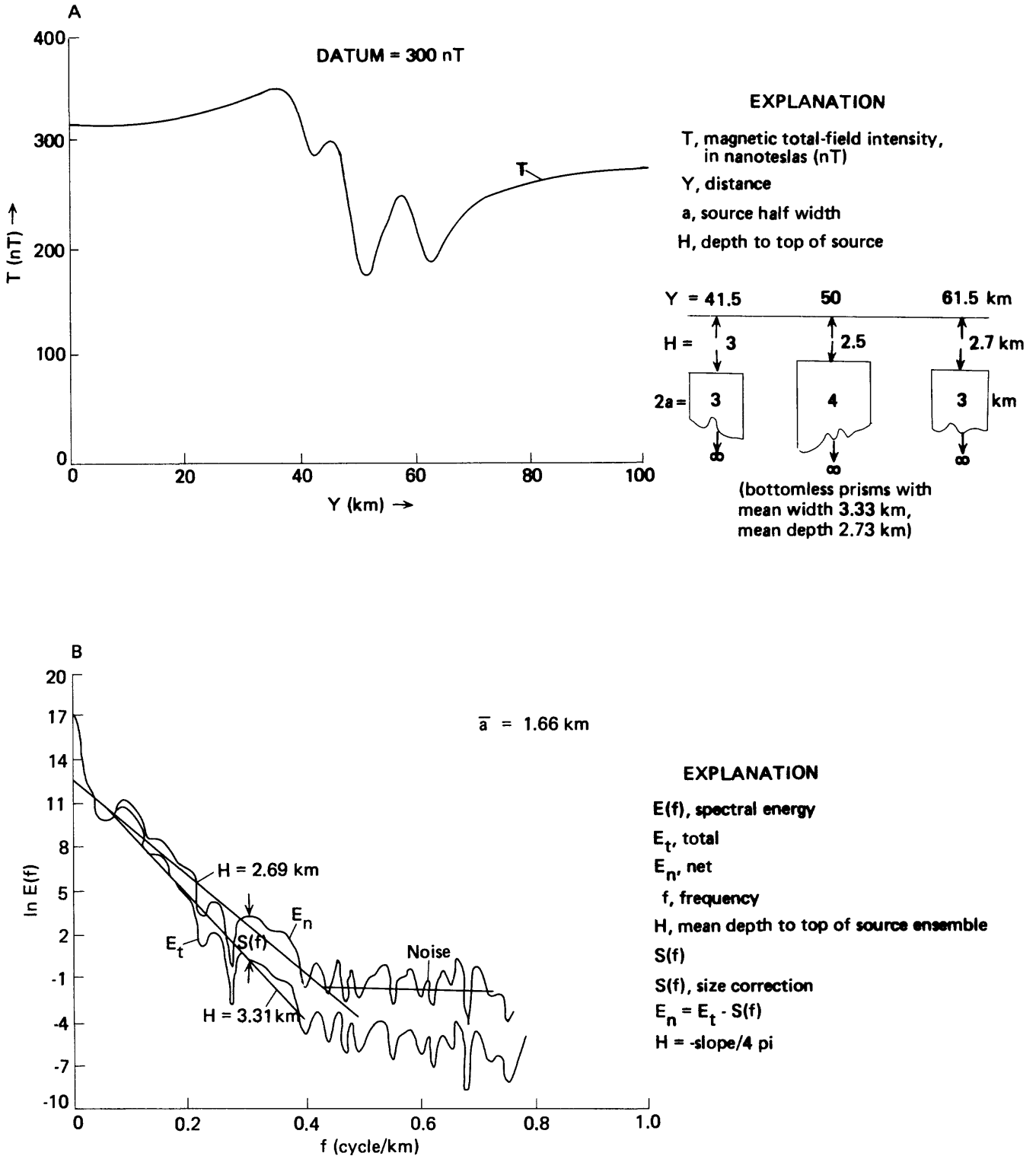

Figure 5.--Spectral analysis of anomalous field due to ensemble of magnetic test models. A, Space domain. B, Frequency domain.

Simple gravity model

We have included a synthetic gravity case in the suite of examples to demonstrate the general applicability of the spectral method of depth estimation to other types of potential field profiles. In this example the assumed model is a bottomless vertical cylinder (fig. 6A) with density contrast -0.1 g/cm^3, diameter 8 km, and top at depth 1.25 km. The same procedure of analysis has been carried out and the energy analyses are presented in figure 6B. The energy contribution due to the model is distinguishable in the frequency range 0.03 to 0.52 cycle/km. In this frequency range the slope of the E_t gives a calculated depth of 1.58 km, or about 27 percent too large. On the other hand, the E_n curve for an anomaly half width of 4 km gives a calculated depth value of 1.21 km, which is within 4 percent of the actual value.

Aeromagnetic profile over Harrat Rahat, western Saudi Arabia

Harrat Rahat is one of the largest Cenozoic lava fields on the Precambrian shield of western Saudi Arabia, extending approximately 300 km south from the outskirts of the city of Al Madinah. In 1976 the major portion of the lava plateau was covered by an aeromagnetic survey along northwest-southeast-trending profiles at 2.5-km spacing and nominal ground clearance of 300 m. The total-intensity aeromagnetic data along each profile, digitally recorded at intervals of approximately 0.07 km, were subjected to systematic depth interpretation using the software described here (Blank and Sadek, 1983). For this purpose the profiles were subdivided into increments of nominal length 20 or 40 km, and the computed energy spectrum for each increment was used to estimate depths to the tops of ensembles of magnetized sources. The objective was to estimate the thickness of the lava series and to construct an isopach map of cover on the basement. We shall discuss three different examples of the spectral analysis and depth determinations.

Line 6, segment 2

This segment of Line 6 is about 25 km long and is located over the southwestern part of the harrat near lat 22°15' N., long 40°10' E. The direction of the flight line is northwest to southeast. Here fresh basaltic lava flows overlie Precambrian metarhyolite, which crops out at the western margin of the harrat. Subroutine "FRQAN" has been applied to the aeromagnetic data and the results are shown in figure 7. It is clear from the total-intensity profile that the magnetic field is nearly flat except for short-wavelength (high-frequency) anomalies produced by the lava flows. The

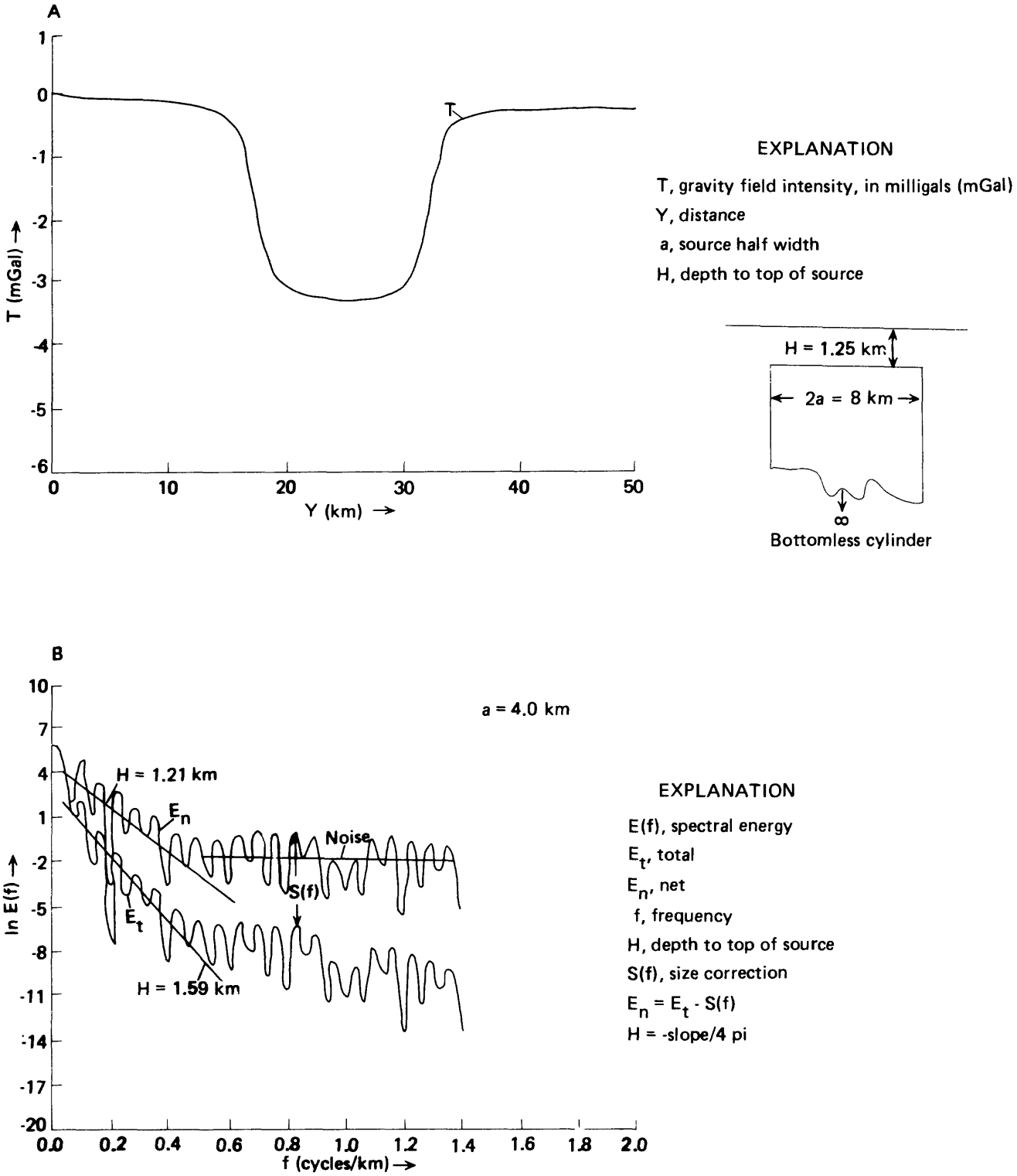

Figure 6.--Spectral analysis of gravity field produced by simple test model. A, Space domain. B, Frequency domain.

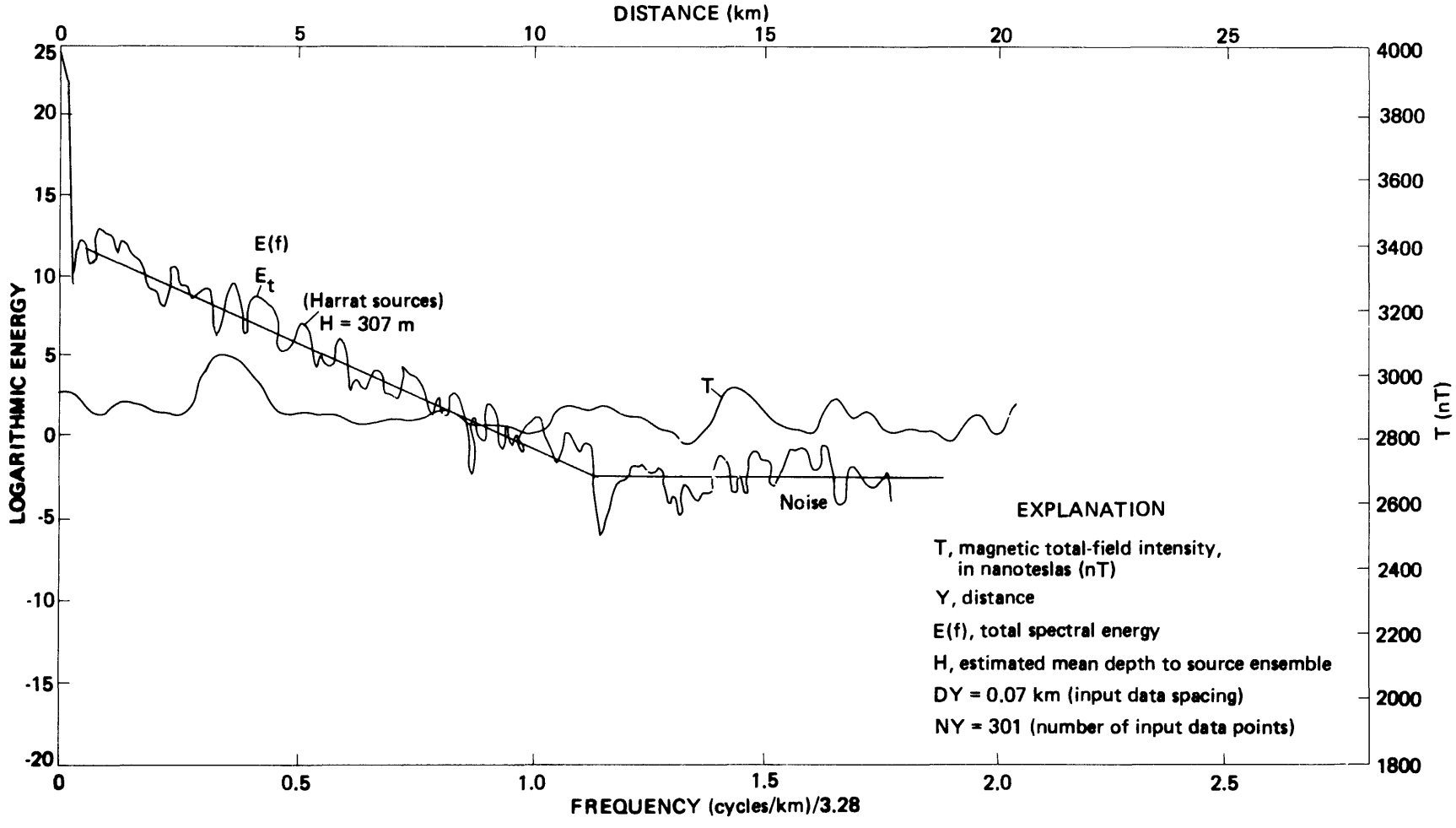

Figure 7.--Spectral analysis of Line 6, segment 2, aeromagnetic survey of Harrat Rahat, Kingdom of Saudi Arabia.

average half width of these anomalies does not exceed the flight height, and therefore no size correction has been applied to the computed spectrum. Examination of the E_t curve shows that it is markedly linear in the frequency range 0.15 to 3.41 cycle/km. The slope of a line fitted to this interval gives a calculated average depth of 307 m to the magnetized sources, which is very close to the average flight height (302 m) registered by the radioaltimeter. Thus the only depth that can be calculated from the E_t curve is interpreted as the depth to the top of the exposed lavas. Since the basement metarhyolites have no magnetic expression, the depth to the Precambrian surface and hence the thickness of the lava series could not be determined from this profile.

Line 33, segment 4

This segment of Line 33 is about 43 km long and located over the western part of Harrat Rahat near lat 23°00' N., long 40°10' E. The flight direction is southeast to northwest. No basement rocks are exposed on the line of traverse. The total magnetic field (T) and the computed energy spectrum (E_t) are illustrated in figure 8. In several parts of the field-intensity profile, it is clear that short-wavelength anomalies are superimposed on anomalies of relatively longer wavelength. The short-wavelength anomalies are due to shallow sources in the Cenozoic lava series, while the longer wavelength anomalies reflect mainly the contribution of basement rocks. The corresponding energy contributions are easily distinguishable on the E_t curve as linear decay intervals in the frequency ranges from 0.9 to 4.0 and 0.06 to 0.9 cycle/km, respectively. From the slopes of these intervals, the calculated average depths to tops of sources in the two ensembles are 297 m and 569 m. The depth 297 m is very close to the average flight height (311 m) registered by the radioaltimeter and thus is the depth to the harrat surface. On the other hand, the depth 569 m, which represents the average depth to the top of sources in a second ensemble, is probably the surface of the underlying basement. Assuming that the volcanic flows directly overlie basement rocks, the difference between the two depths (272 m) is the thickness of the lava series.

Line 37, segment over drill hole SAH-20

This example provides a direct comparison between a basement depth estimate from spectral analysis with the actual depth determined in a drill hole. Line 37 passes almost over the position of ground-water exploration drill hole SAH-25 (Torrent, 1976). A segment of profile centered over the hole was selected for analysis; the segment contains 501 data points spaced at 70 m (total length 35 km). The logarithmic spectral energy-decay curve (fig. 9) yields an estimated average depth to a shallow source ensemble (the harrat

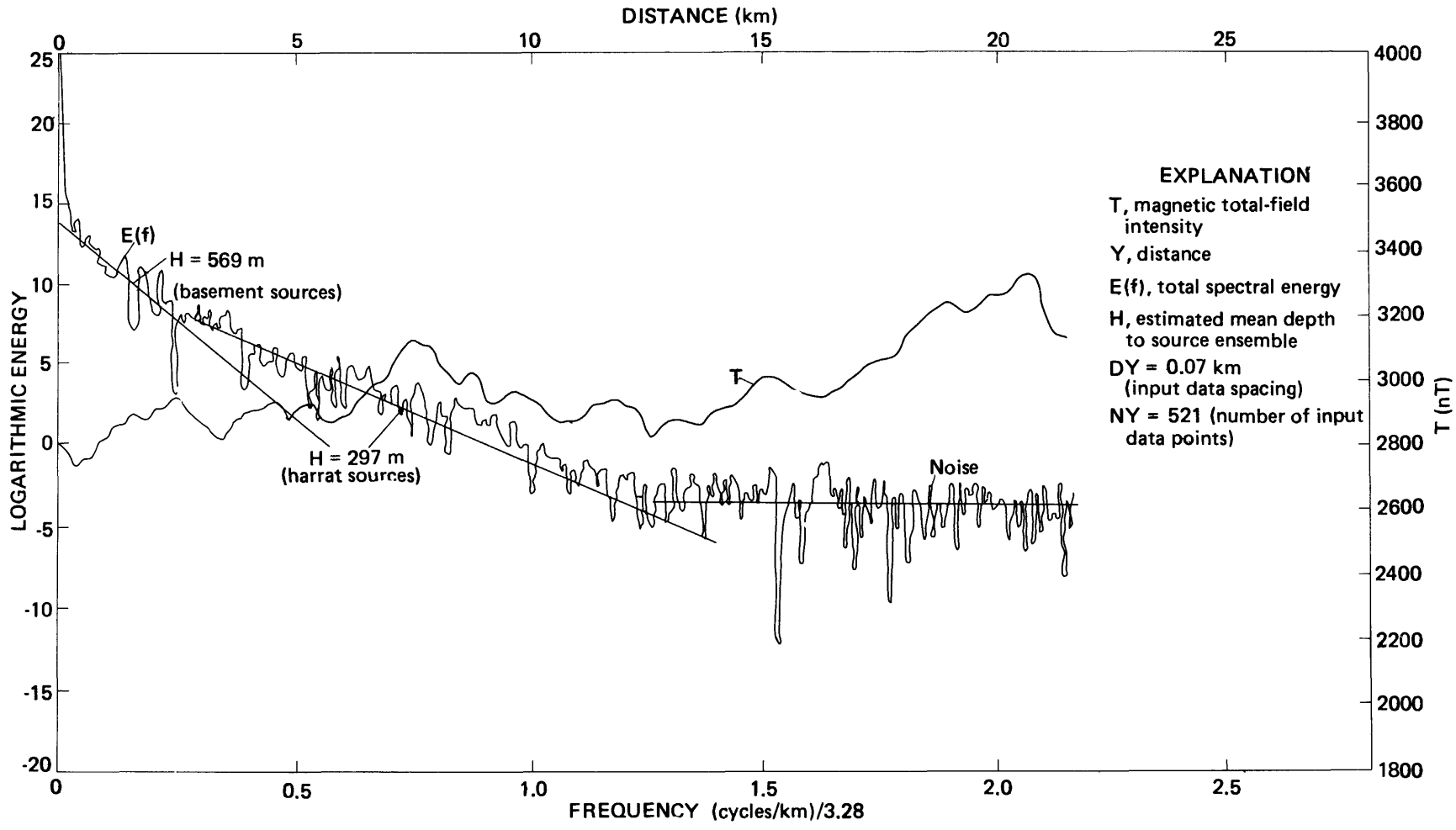

Figure 8.--Spectral analysis of Line 33, segment 4, aeromagnetic survey of Harrat Rahat, Kingdom of Saudi Arabia.

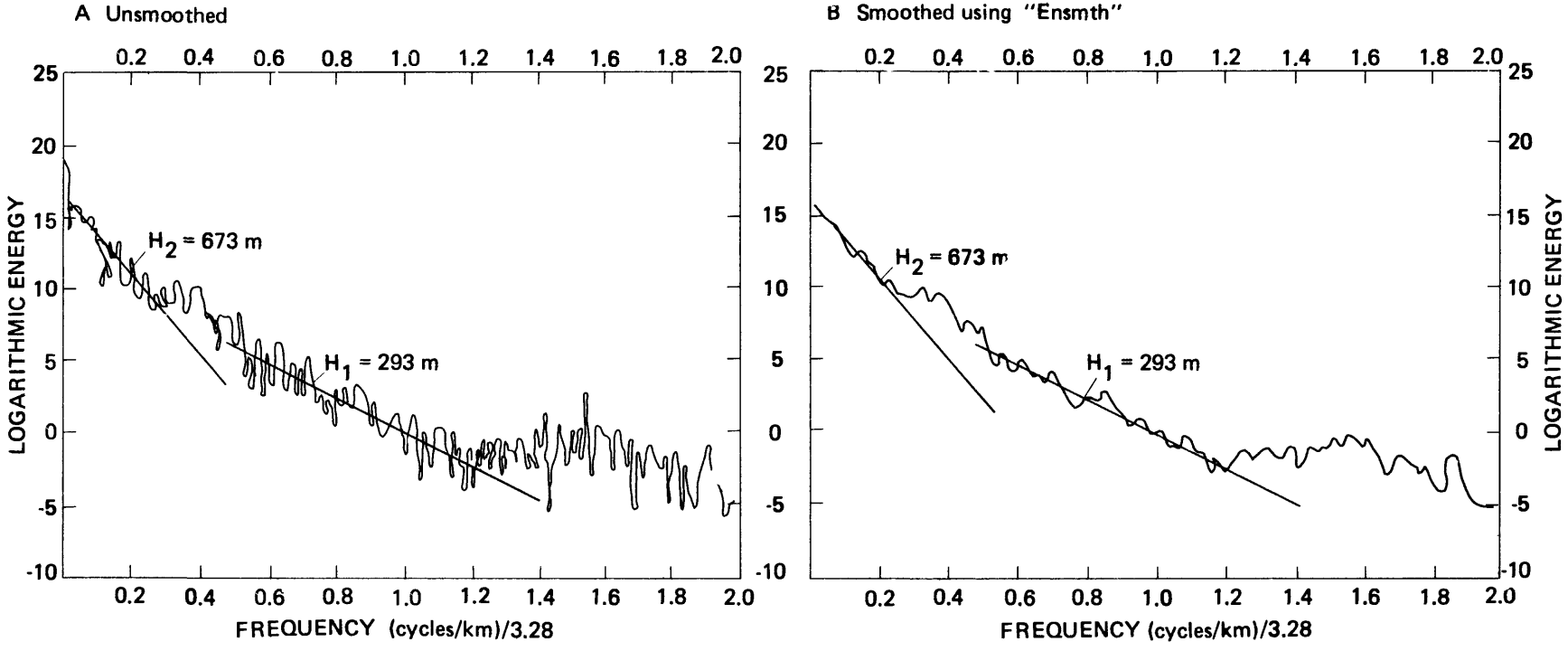

Figure 9.--A, Unsmoothed and B, smoothed energy spectrum for segment of total-intensity aeromagnetic profile (Line 37) centered over diamond drill hole SAH-25, Harrat Rahat. Length of segment is 35 km; NY=501 points, NF=251 points. H1 and H2 are estimated depths to surface of harrat and basement, respectively. H_2-H_1 = 380 m from spectra; depth to basement is 362 m in drill hole. "ENSMTH" is 7-point triangular filter subroutine (see text).

surface) of 293 m, or about the nominal terrain clearance, while the estimated depth to a deeper source ensemble (Precambrian basement) is 673 m, so that the estimated thickness of cover is 380 m. The depth to basement proved by the drill hole is 362 m. The excellent agreement of the spectral depth estimates with the drilling result (only 5 percent error) is better than could be expected, as there is known to be considerable relief on the concealed basement surface, and even though the spectral estimates are center weighted, they are influenced by depths of all sources distributed beneath the entire 35-km-long segment of profile analyzed. Furthermore, size corrections for the deeper sources might be expected to reduce the estimate by more than the magnitude of the discrepancy. Figure 9 also illustrates application of the smoothing subroutine "ENSMTH".

Aeromagnetic profile at Diyur, Western Desert of Egypt

The Diyur aeromagnetic anomaly is a basement feature delineated during petroleum exploration surveys of the Western Desert of Egypt (fig. 10). In the vicinity of the anomaly, which is centered at about lat 29°17' N., long 28°34' E., basement rocks are concealed beneath a nonmagnetic Tertiary cover known from drilling data to be about 1.5 km thick. The aeromagnetic data were digitized at 0.5-km intervals along a south-north profile bisecting the anomaly. The total-intensity profile of figure 10A shows a large central high with a half width of about 15 km. Spectral analysis of this profile included the application of subroutine "FRQAN" (E_t curve) and size correction using "CSIZE" (E_n curve). The energy contribution of the magnetic anomaly is easily distinguished in the frequency range 0.05 to 0.4 cycle/km. The corresponding slope of the E_t curve gives a depth of 2.24 km, which is about 46 percent greater than the depth given by drilling. In the same frequency range, using the anomaly half width of 4.0 km (measured between points of inflection) to compute the size correction, a depth value of 1.63 km is obtained from the slope of the E_n curve. This value is still an overestimation but now is only about 7 percent greater than the actual value at the drill site.

It can be seen that the energy curve has a "hump" in the frequency range 0.2 to 0.3 cycle/km. This hump is attributable to a sheetlike source body within the cover rock sequence. The actual depth of this additional source cannot be estimated from the energy curve because of the relatively large digitization interval of the total magnetic field intensity profile used to produce the energy curve. However, small irregularities observed in the total-intensity curve (fig. 10) probably also reflect the same shallower source. The source is believed to be a layer of volcanic rocks that extends from Cairo in the east to Bahariyya Oasis in the west (Meshref and others, 1980).

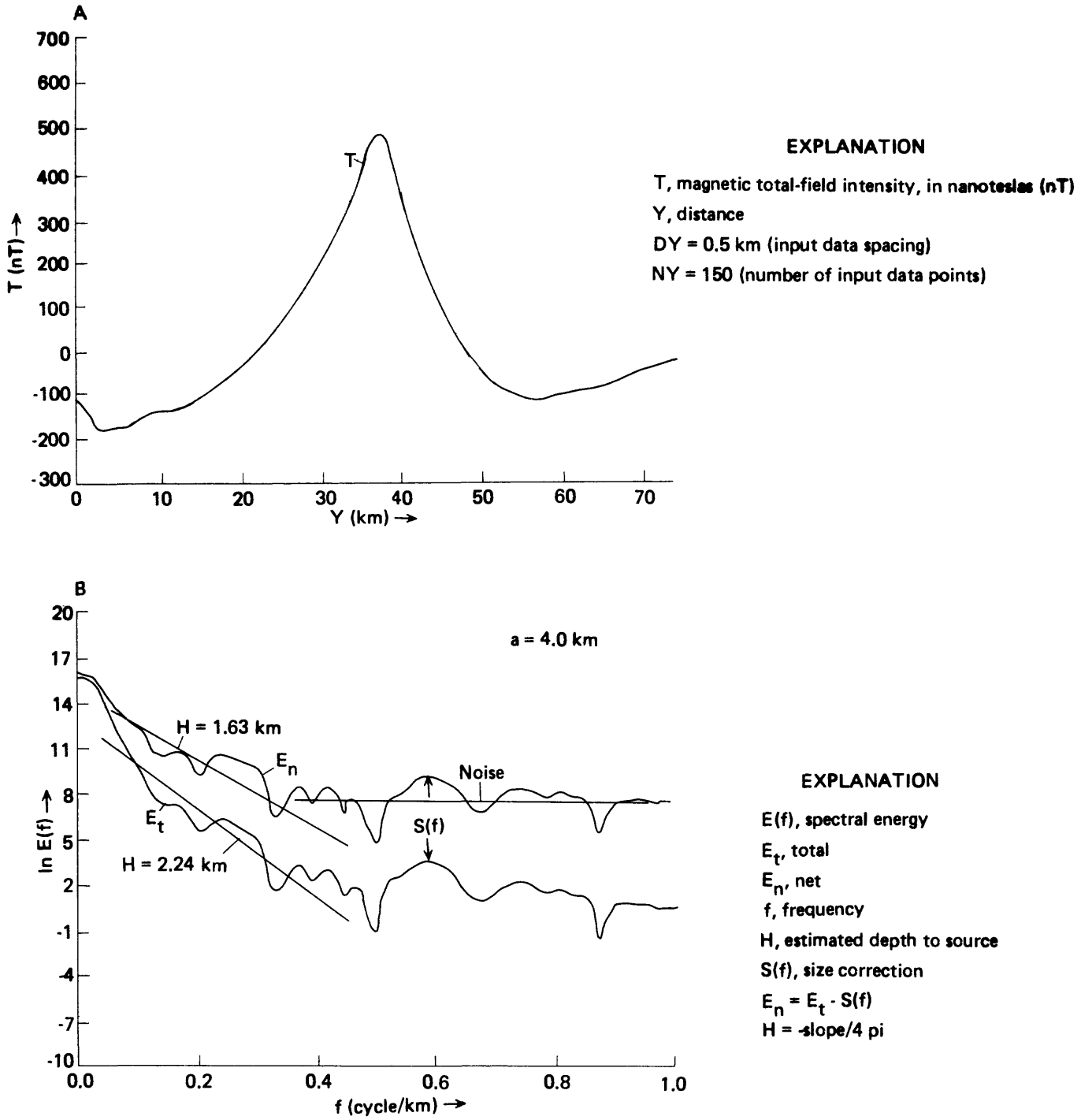

Figure 10.--Spectral analysis of aeromagnetic profile across Diyur area, Western Desert of Egypt. A, Space domain. B, Frequency domain. Estimated depth to anomaly source is 1.63 km after size correction; proved depth to basement in vicinity of anomaly is 1.53 km from drilling.

CONCLUSIONS

The foregoing examples attest to the effectiveness of the spectral method of depth estimation for a variety of synthetic and real profiles. The method must be applied with caution, however, in consideration of important constraints that affect the validity of the analyses. We summarize the main points as follows:

1. Analysis of the spectrum is restricted to a finite frequency interval. The practical lower limit is determined by the finite length of profile, which in practice means that the maximum depth that can be determined is at most about one-quarter or even one-fifth of the profile length. The upper limit is set by noise due to round-off error in the recorded data and can never exceed the Nyquist frequency. The data should represent field-intensity samples at a sufficiently fine interval for spectral aliasing to be minimized (that is, no "spikes" should be present; only low-energy noise is reflected). In practice this requires that the sample interval be no larger than about one-quarter of the width of the smallest anomalies present (Spector, 1968). Best results are obtained when the data have been detrended (a linear regional gradient has been removed).

2. The assumption of bidimensionality of sources, implicit in the one-dimensional computation of the spectrum for a profile, does not adversely affect the profile depth estimates provided the distribution of sources in the horizontal plane is such that the radial spectrum is independent of the azimuthal angle θ. This situation strictly applies only when sources are small, numerous, equidimensional in the horizontal plane, and randomly distributed. However, in many situations encountered in practice, the depth factor is probably very close to the same whether the sources are considered two dimensional or three dimensional. But if the field-intensity data indicate that the sources are indeed predominantly two dimensional, then the profile must be normal to the strike direction (we note, as an extreme example, that the energy is limited to zero frequency for profiles parallel to the strike).

3. The energy spectrum of a wide variety of simple source configurations can be expressed as the product of six factors, only three of which are functions of frequency (or wave number): the depth factor, the horizontal size (width) factor, and the vertical size (depth extent or vertical thickness) factor. Estimation of the depth h is essentially independent of source magnetization and orientation of the earth's field; knowledge of the absolute level of the spectral energy is not required.

4. The logarithmic spectral decay rate is dominated by the depth term, which is simply $-4\pi fh$ or $-2rh$. When the other two factors are negligible or have been compensated, the depth to the top of a source or the average depth to the tops of sources in an ensemble is obtained simply by measuring the slope of the decay curve. If two or more ensembles are present, each with a characteristic mean depth, each will produce a linear decay interval in a different part of the spectrum.

5. The finite horizontal cross section of sources increasingly steepens the logarithmic energy-decay rate as horizontal dimensions increase relative to depth. The steepening is most drastic at low frequencies. In general, this effect must be compensated in order to avoid serious overestimation of depths. An adequate correction, or spectral "refinement", requires only a rough knowledge of the source dimensions and is relatively insensitive to source shape.

6. By the presence or absence of a logarithmic energy maximum at a nonzero frequency, the spectrum will immediately reveal whether sources are depth limited. For sources with depth extent (vertical thickness) much less than the depth to the top, the depth can be estimated through further refinement of the spectrum by subtracting a term $\ln r^2$ from the logarithmic energy and then fitting a straight line to the remainder, or, if the maximum is well defined, by use of the relationship $r=1/h$. If the depth extent of a source body exceeds the depth to its top, the spectrum is nearly that of a bottomless source. The depth estimate is generally much more satisfactory than the estimate of depth extent.

7. The effect of vertical dispersion of sources is negligible if the depth variations are within about 25 percent of the mean depth. In practice it appears that sources in crystalline terranes have relatively large depth extent and therefore the ensemble depth for a crystalline basement is close to the mean depth to the basement surface.

8. Horizontal dispersion of sources affects only the phase of the complex amplitude spectrum, and not the energy spectrum. If the depth to a single dominant source is desired, the estimate can sometimes be improved by centering the profile over the associated amplitude anomaly.

As we remarked at the onset, frequency analysis of profile data has many applications in addition to depth estimation. Several of these, such as computation of derivatives and frequency stripping (band-pass filtering), can be used to improve the quality of the depth estimates themselves. For a discussion of these techniques the reader

should consult especially the works of Green (1972) and Spector and Parker (1979).

In view of the enormous amount of potential-field data now available for Saudi Arabia, particularly aeromagnetic data over the Arabian Shield and adjacent Cover Rock, it is to be hoped that this review of the spectral method and presentation of software can contribute to the task of analysis, and that not only spectral depth estimation, but other operations in the frequency domain will in the future be more widely applied. The profile technique may be especially useful where profiles are relatively widely spaced and the data are not directly amenable to contouring.

ACKNOWLEDGMENTS

The work reported here has been carried out in accordance with an agreement between the U.S. Geological Survey and the Saudi Arabian Ministry of Petroleum and Mineral Resources. We gratefully acknowledge the assistance provided by staff of the Bureau de Recherches Geologiques et Minieres (BRGM), Saudi Arabian Mission, especially Mr. J. M. Georgel, Deputy Director, who kindly consented to our use of the BRGM computing facilities, and Mr. J. Bobillier, who made available the plotting routine used to display all data from Harrat Rahat. For the theoretical development and methods of numerical integration we have borrowed heavily from the works of A. Spector. We thank Mark E. Gettings for a thoughtful review of the original manuscript.

DATA STORAGE

Data-file USGS-DF-04-24 was established for the storage of data used in this report. No entries were made to the Mineral Occurrences Documentation System (MODS) in connection with this report.

REFERENCES CITED

Alldredge, L. R., Van Voorhis, G. D. and Davis, T. M., 1963, A magnetic profile around the world: Journal of Geophysical Research, v. 68, p. 3679-3692.

Bhattacharyya, B. K., 1966, Two-dimensional harmonic analysis as a tool for magnetic interpretation: Geophysics, v. 30, p. 829-875.

_____, 1967, Some general properties of potential fields in space and frequency domains - A review: Geoexploration, v. 5, p. 127-143.

Bhismasankaram, V. L. S., Mohan, N. L., and Rao, S. V. S., 1977, Analysis of gravity effect of two-dimensional trapezoidal prisms using Fourier transforms: Geophysical Prospecting, v. 25, p. 334-341.

Blank, H. R., and Sadek, H. S., 1983, Spectral analysis of the 1976 aeromagnetic survey of Harrat Rahat, Kingdom of Saudi Arabia: Saudi Arabian Deputy Ministry for Mineral Resources Open-File Report, USGS-OF-03-67, 29 p.; also, 1983, U.S. Geological Survey Open-File Report 83-640.

Cassano, E., and Rocca, F., 1975: Interpretation of magnetic anomalies using spectral estimation techniques: Geophysical Prospecting, v. 23, no. 4, p. 663-681.

Chowdary, V. M. R., 1978, Spectral analysis of total magnetic anomalies of step model (short note): Geophysics, v. 43, no. 3, p. 634-636.

Cooley, J. W., and Tukey, J. W., 1965, An algorithm for the machine calculation of complex Fourier series: Journal of Mathematics of Computation, v. 19, p. 297-301.

Cordell, L., and Grauch, V. J., 1982, Reconciliation of the discrete and integral Fourier transforms: Geophysics, v. 47, p. 237-243.

Curtis, C. E., and Jain, S., 1975, Determination of volcanic thickness and underlying structures from aeromagnetic maps in the Silet area of Algeria: Geophysics, v. 40, p. 79-90.

Dean, W., 1958, Frequency analysis for gravity and magnetic interpretation: Geophysics, v. 23, p. 97-127.

Green, A. G., 1972, Magnetic profile analysis: Geophysical Journal Royal Astronomical Society, v. 30, p. 393-403.

Horton, C. W., Hempkins, B., Hoffman, A. A. J., 1964, A statistical analysis of some aeromagnetic maps from the northwestern Canadian shield, Geophysics, v. 29, p. 582-601.

Meshref, W. M., Refai, E. M., Sadek, H. S., Abdel-Baki, S. H., El-Sirafy, A. M., El-Kattan, E. I., El-Meliegy, M. A., and El-Sheikh, M. M., 1980, Structural geophysical interpretation of basement rocks of the northwestern desert of Egypt: Geological Survey of Egypt, Annals, v. 10, p. 923-937.

Pedersen, L. B., 1978a, Wave number domain expressions for potential fields from arbitrary 2-, 2 $^{1}/_{2}$-, and 3-dimensional bodies: Geophysics, v. 43, p. 626-630.

_____, 1978b, A statistical analysis of potential fields using a vertical circular cylinder and a dike: Geophysics, v. 43, p. 943-953.

Rao, K. G. C., and Avasthi, D. N., 1973, Analysis of the Fourier spectrum of the gravity effect due to two-dimensional triangular prism: Geophysical Prospecting, v. 21, p. 526-542.

Regan, R. D. and Hinze, W. J., 1977, Fourier transforms of finite-length theoretical gravity anomalies: Geophysics, v. 42, p. 1450-1475.

_____, 1978, Theoretical transforms of the gravity anomalies of two idealized bodies: Geophysics, v. 43, p. 631-633.

Sadek, H. S., 1978, Relation between geology and aerial radiometry of the Abu Awayel area, Eastern Desert of Egypt, corroborated by aeromagnetic survey: Cairo University, Ph.D. thesis, 284 p.

Sadek, H. S., Meshref, W. M., Abdel-Hadi, H. M., and Soliman, S. A., *in press*, Geophysical investigations in the Precambrian rocks of Wadi Allaqi, Southeastern Desert of Egypt: Faculty of Earth Sciences, King Abdul Aziz University, Bulletin No. 6.

Serson, P. H., and Hannaford, W. L. W., 1957, A statistical analysis of magnetic profiles: Journal of Geophysical Research, v. 62, p. 1-18.

Spector, A., 1968, Spectral analysis of aeromagnetic data: Toronto University, Ph.D. thesis, 239 p.

Spector, A., and Bhattacharyya, B. K., 1966, Energy density spectrum and autocorrelation function of anomalies due to simple magnetic models: Geophysical Prospecting, v. 14, p. 242-272.

Spector, A., and Grant, F. S., 1970, Statistical models for interpreting aeromagnetic data: Geophysics, v. 35, p. 293-302.

Spector, A., and Parker, W., 1979, Computer compilation and interpretation of geophysical data, in Hood, P. J., ed., Geophysics and geochemistry in the search for metallic ores: Geological Survey of Canada, Economic Geology Report 31, p. 527-544.

Torrent, H., 1976, Jabal Sayid water supply, part I, Hydrogeology of the Harrat Rahat basalt: Bureau de Recherches Geologiques et Minieres (Saudi Arabian Mission) Report 76-JED-8, 60 p.

Tranter, C. J., 1962, Integral transforms in mathematical physics: Methuen Monograph, 129 p.

APPENDIX A

APPENDIX A: SUBROUTINE "FRQAN"

Subroutine "FRQAN" is written in FORTRAN IV. Input can be any potential-field intensity data as a function of distance along a profile, and output is logarithmic (base e) energy (dimensionless) as a function of frequency measured in reciprocal distance units (for example, cycles per km). A flow chart is provided. The program follows.

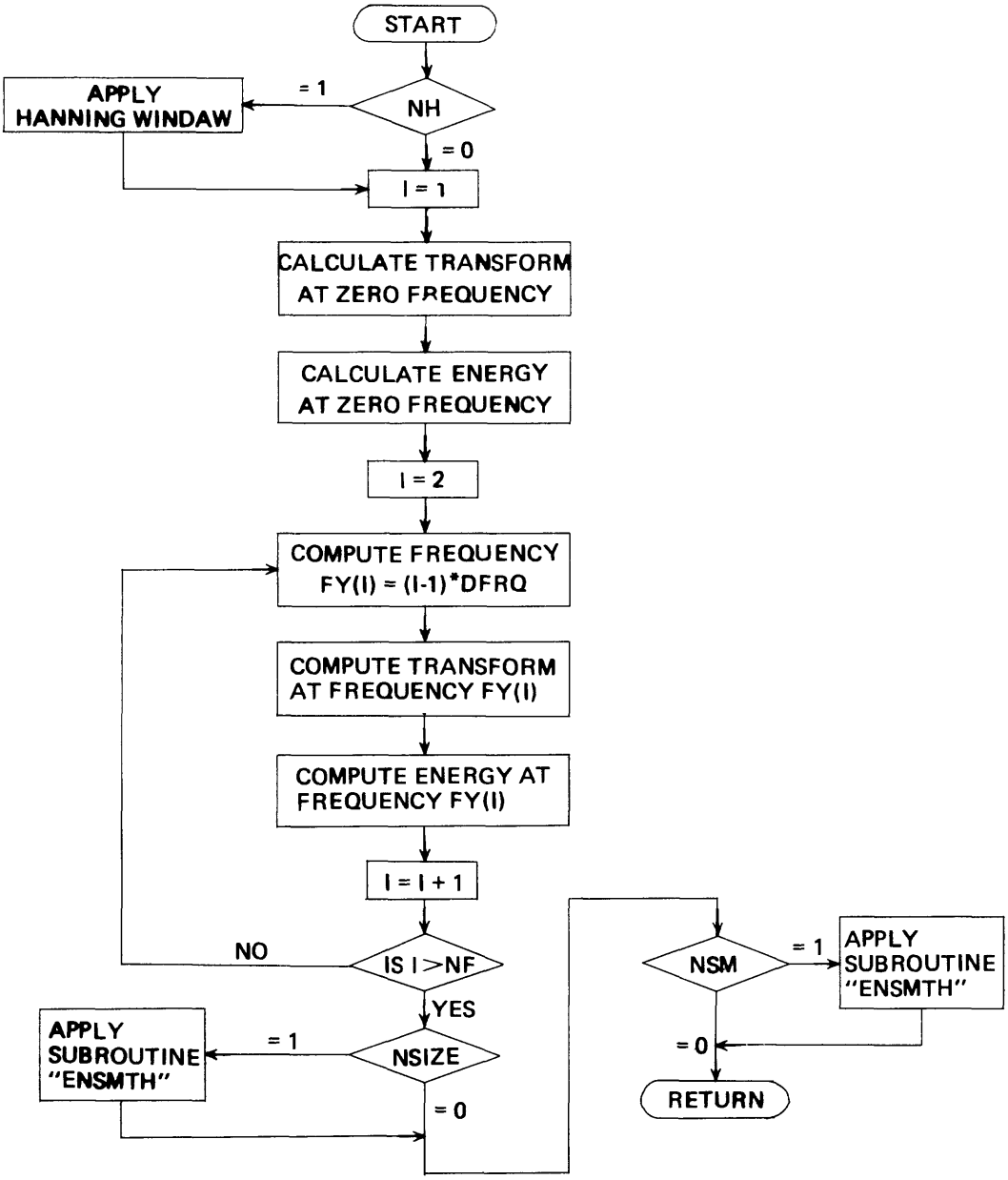
START
NH
= 1
APPLY HANNING WINDAW
= 0
I = 1
CALCULATE TRANSFORM AT ZERO FREQUENCY
CALCULATE ENERGY AT ZERO FREQUENCY
I = 2
COMPUTE FREQUENCY FY(I) = (I-1)*DFRQ
COMPUTE TRANSFORM AT FREQUENCY FY(I)
COMPUTE ENERGY AT FREQUENCY FY(I)
I = I + 1
IS I >NF
NO
YES
NSIZE
= 1
APPLY SUBROUTINE "ENSMTH"
= 0
NSM
= 1
APPLY SUBROUTINE "ENSMTH"
= 0
RETURN

```
!       FRQAN.FTN                                          14-DEC-83 10:22:36
!       ------------------------------------------------------------------------
!       C**************************************************************************
!       C     THIS SUBROUTINE COMPUTES   FREQUENCY AND CORRESPONDING
!       C     ENERGY SPECTRUM OF EQUALLY SPACED POTENTIAL FIELD DATA
!       C     DIGITIZED ALONG A GIVEN PROFILE. THE (I/O) QUANTITIES ARE:
!       C     A- NUMERIC CONSTANTS
!       C        1- NY      NUMBER OF INPUT DATA POINTS
!       C        2- DY      INPUT DATA INTERVAL
!       C        3- NH      = 1  APPLY HANNING WINDOW
!       C                   = 0  NO HANNING WINDOW IS APPLIED
!       C        4-NSIZE    = 1  APPLY SIZE CORRECTION
!       C                   = 0  NO SIZE CORRECTION
!       C        5-HWD      AVERAGE HALF WIDTH OF SOURCE OR ENSEMBLE
!       C                   ( HWD=0.0 IF NO SIZE CORRECTION IS NEEDED)
!       C        6-NSM      = 1  SMOOTH THE OUTPUT ENERGY CURVE
!       C                   = 0  NO SMOOTHING OF THE OUTPUT ENERGY CURVE
!       C        7- FRQN    OUTPUT NYQUIST FREQUENCY
!       C        8- DFRQ    OUTPUT FREQUENCY INTERVAL
!       C        9- NF      NUMBER OF OUTPUT ENERGY POINTS
!       C     B- ARRAYS
!       C        1- DT      ARRAY OF INPUT POTENTIAL FIELD DATA
!       C        2- ES      ARRAY OF OUTPUT LN(ENERGY) SPECTRUM DATA
!       C        3- FY      ARRAY OF OUTPUT FREQUENCY VALUES
!       C        4- A       ARRAY OF OUTPUT REAL VALUES OF THE TRANSFORM
!       C        5- B       ARRAY OF OUTPUT IMAGINARY VALUES OF THE TRANSFORM
!       C**************************************************************************
!             SUBROUTINE FRQAN(NY,DY,HWD,NH,NSIZE,NSM,DT,A,B,NF,FRQN,DFRQ,FY,ES)
!             DIMENSION DT(NY),A(NY),B(NY),ES(NY),FY(NY),FC(7)
!             PI=4.*ATAN(1.)
!       C
!       C     CALCULATE SPACE DOMAIN PARAMETERS
!       C
!             YL=(NY-1)*DY
!             LY=YL
!             N1=(NY-3)/2
!             N2=(NY-1)/2
!             IF (NH .EQ. 0) GO TO 100
!       C
!       C     APPLY HANNING WINDOW
!       C
!             DO 100 I=1,NY
!             Y=(I-1)*DY-YL/2.
!             Q=0.5*(1.+COS(2.*PI*Y/YL))
!             DT(I)=DT(I)*Q
!       100   CONTINUE
!       C
!       C     CALCULATE PARAMETERS OF FREQUENCY DOMAIN
!       C
!             DFRQ=1./YL
!             FRQN=1./(2.*DY)
!             NF=FRQN/DFRQ
!       C
!       C     CALCULATE ENERGY AT ZERO FREQUENCY
!       C
!             SUM1=0.0
!             DO 110 K=1,N1
!             I1=2*K+1
!       110   SUM1=SUM1+DT(I1)
```

```
!               SUM2=0.0
!               DO 120 K=1,N2
!         120   SUM2=SUM2+DT(2*K)
!               A(1)=(DY/3.)*(2.*SUM1+4.*SUM2+DT(1)+DT(NY))
!               B(1)=0.0
!               FY(1)=0.0
!               ES1=A(1)*A(1)
!               ES(1)=ALOG(ES1)
!         C
!         C     CALCULATE ENERGY AT DIFFERENT FREQUENCIES
!         C
!               DO 200 J=2,NF
!               FY(J)=(J-1)*DFRQ
!               CE=0.0
!               SE=0.0
!               CT=0.0
!               ST=0.0
!               V=2.*PI*FY(J)
!               Z=V*DY
!               CV=COS(V*YL/2.)
!               SV=SIN(V*YL/2.)
!               CZ=COS(Z)
!               SZ=SIN(Z)
!               ALP=1./Z+(CZ*SZ/(Z*Z))-(2.*SZ*SZ/Z**3.)
!               BET=2.*((1.+CZ*CZ)/(Z*Z)-2.*CZ*SZ/Z**3.)
!               GAM=4.*(SZ-Z*CZ)/Z**3.
!               DO 210 K=1,N1
!               I1=2*K+1
!               AA=2.*K*DY-YL/2.
!               CE=CE+DT(I1)*COS(V*AA)
!               SE=SE+DT(I1)*SIN(V*AA)
!         210   CONTINUE
!               CE=CE+0.5*(DT(NY)+DT(1))*CV
!               SE=SE+0.5*(DT(NY)-DT(1))*SV
!               DO 220 K=1,N2
!               BB=(2.*K-1.)*DY-YL/2.
!               CT=CT+DT(2*K)*COS(V*BB)
!               ST=ST+DT(2*K)*SIN(V*BB)
!         220   CONTINUE
!               A(J)=DY*(ALP*(DT(NY)+DT(1))*SV+BET*CE+GAM*CT)
!               B(J)=DY*(-ALP*(DT(NY)-DT(1))*CV+BET*SE+GAM*ST)
!               ES1=A(J)*A(J)+B(J)*B(J)
!               ES(J)=ALOG(ES1)
!         200   CONTINUE
!               IF(NSIZE .EQ. 0) GO TO 230
!         C
!         C     APPLY SIZE CORRECTION
!         C
!               CALL CSIZE(NF,HWD,FY,ES,DT)
!         230   IF(NSM .EQ. 0) GO TO 240
!         C
!         C     SMOOTH THE OUTPUT ENERGY CURVE
!         C
!               CALL ENSMTH(NF,ES)
!         240   RETURN
```

APPENDIX B

APPENDIX B: SUBROUTINE "CSIZE"

Subroutine "CSIZE", also written in FORTRAN IV, is entered from subroutine "FRQAN" if the calling option has been exercised. A value of average half width of sources must be provided in the "FRQAN" input. A flow chart is provided. The program follows.

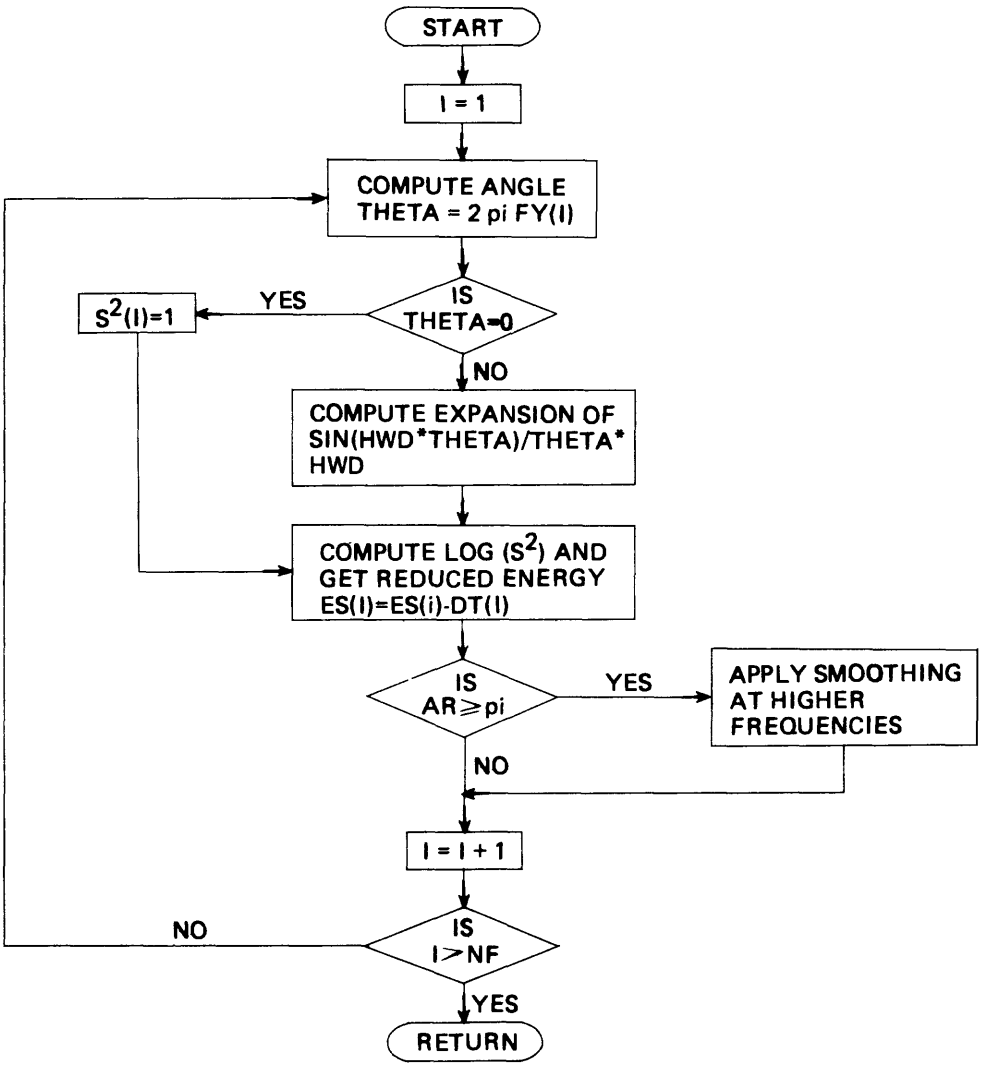
START
I = 1
COMPUTE ANGLE
THETA = 2 pi FY(I)
IS
THETA=0
YES
S²(I)=1
NO
COMPUTE EXPANSION OF
SIN(HWD*THETA)/THETA*
HWD
COMPUTE LOG (S²) AND
GET REDUCED ENERGY
ES(I)=ES(i)-DT(I)
IS
AR≥pi
YES
APPLY SMOOTHING
AT HIGHER
FREQUENCIES
NO
I = I + 1
IS
I>NF
NO
YES
RETURN

```
!       CSIZE.FTN                                          14-DEC-83 10:23:44
!       ------------------------------------------------------------------------
!       C*****************************************************************
!       C     SUBROUTINE 'CSIZE' INTODUCES FINITE SIZE CORRECTIONS
!       C     TO THE ENERGY SPECRUM OF POTENTIAL FIELD DATA
!       C     COMPUTED USING SUBROUTINE 'FRQAN'
!       C
!       C     THE (I/O) QUANTITIES ARE:
!       C     A- NUMERIC CONSTANTS   *
!       C        1- NF      NUMBER OF INPUT FREQUENCY POINTS
!       C        2- HWD     AVERAGE HALF WIDTH OF SOURCE OR ENSEMBLE
!       C     B- ARRAYS
!       C        1- FY      ARRAY OF INPUT FREQUENCY VALUES
!       C        2- ES      ARRAY OF INPUT LN(ENERGY) VALUES AND
!       C                   OUTPUT CORRECTED LN(ENERGY) VALUES
!       C        3- DT      ARRAY OF OUTPUT SIZE CORRECTION FACTOR
!       C*****************************************************************
!             SUBROUTINE CSIZE(NF,HWD,FY,ES,DT)
!             DIMENSION FY(NF),ES(NF),DT(NF)
!             PI=4.*ATAN(1.)
!             DO 100 I=1,NF
!       C
!       C     COMPUTE ANGLE
!       C
!             U=2.*PI*FY(I)
!             THETA=U*HWD
!             IF(THETA .EQ. 0.0) 140
!             IF(THETA .GT. 1.) GO TO 170
!       C
!       C     COMPUTE EXPANSION OF SIN(THETA)/THETA
!       C
!             SUM=0.0
!             L=1
!       110   J=L-1
!             J1=(-1)**J
!             J2=2*J+1
!             Y=THETA**J2
!             SUM1=1
!             DO 120 K=1,J2
!       120   SUM1=SUM1*K
!             VAL=J1*Y/(SUM1*J2)
!             SUM=SUM+VAL
!             IF(ABS(VAL) .LE. 0.001) GO TO 130
!             L=L+1
!             GO TO 110
!       130   VALUE=(SUM/THETA)**2.
!             GO TO 150
!       140   VALUE=1.
!       C
!       C     STORE SIZE CORRECTION VALUES AND REDUCE ENERGY
!       C
```

```
!       150   DT(I)=ALOG(VALUE)
!       160   ES(I)=ES(I)-DT(I)
!       100   CONTINUE
!             RETURN
!       C
!       C     APPLY PEDERSEN FORMULA FOR SIZE CORRECTION
!       C     TO AVOID HIGH FREQUENCY NOISE
!       C
!       170   DO 200 K=I,NF
!             U=2.*PI*FY(K)
!             DT(K)=-2.*ALOG(U)
!             ES(K)=ES(K)-DT(K)
!       200   CONTINUE
!             RETURN
```

APPENDIX C

APPENDIX C: SUBROUTINE "ENSMTH"

Subroutine "ENSMTH" is also written in FORTRAN IV and requires as input only an array of energy points. At present it is contained as the final option in subroutine "FRQAN". A flow chart is provided. The program listing follows.

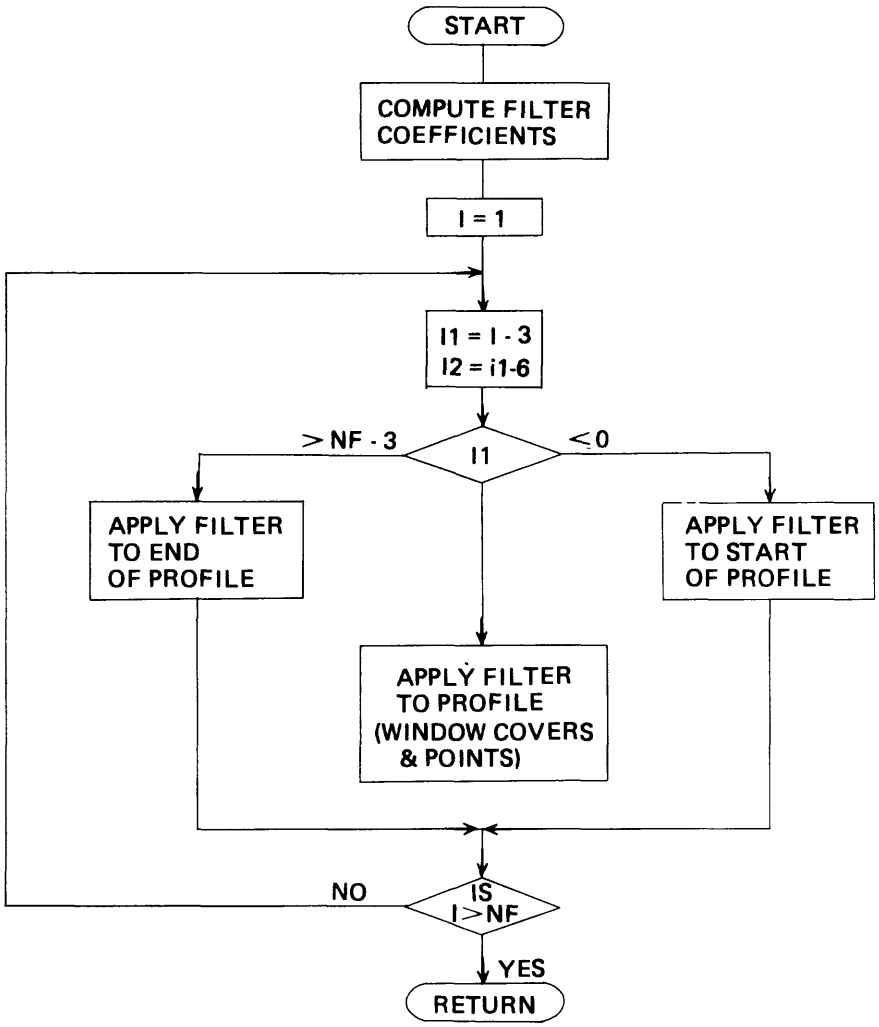
START
COMPUTE FILTER COEFFICIENTS
I = 1
I1 = I - 3
I2 = i1-6
> NF - 3
I1
< 0
APPLY FILTER TO END OF PROFILE
APPLY FILTER TO START OF PROFILE
APPLY FILTER TO PROFILE (WINDOW COVERS & POINTS)
NO
IS I > NF
YES
RETURN

```
!       ENSMTH.FTN                                    14-DEC-83 10:24:30
!       ------------------------------------------------------------------------------
!       C*******************************************************************************
!       C
!       C     THIS SUBROUTINE IS USED TO SMOOTH THE COMPUTED LN(ENERGY) SPECTRUM
!       C     CURVE COMPUTED FROM SUBROUTINE FRQAN   THIS OPERATION IS CARRIED
!       C     OUT USING A TRIANGLE FILTER SET (1/16, 2/16, 3/16, 4/16, 3/16,
!       C     2/16, 1/16) (A.G. GREEN, 1972).
!       C     THE I/O QUANTITIES ARE:
!       C     A- NUMERIC CONSTANTS:
!       C        1- NF     NUMBER OF ENERGY POINTS
!       C     B- ARRAYS:
!       C        1- ES     ARRAY OF INPUT LN(ENERGY) VALUES AND
!       C                  OUTPUT SMOOTHED LN(ENERGY) VALUES
!       C        2- FC     ARRAY OF THE FILTER COEFFICIENT
!       C*******************************************************************************
!             SUBROUTINE ENSMTH(NF,ES)
!             DIMENSION FC(7),ES(NF)
!       C
!       C     COMPUTE FILTER COEFFICIENTS
!       C
!             DO 10 I=1,7
!             IF(I .GT. 4) GO TO 15
!             FC(I)=FLOAT(I)
!             GO TO 10
!       15    FC(I)=8.-I
!       10    CONTINUE
!       C
!       C     APPLY SMOOTHING  FILTER
!       C
!             DO 20 I=1,NF
!             I1=I-3
!             I2=I1+6
!             N=1
!             SUME=0
!             SUMF=0
!       C
!       C     CONDITION FOR MISSING VALUES OF THE
!       C      FILTER AT THE START OF THE PROFILE
!       C
!             IF(I1 .GT. 0) GO TO 25
!             N=2-I1
!             I1=1
!       25    DO 30 J=I1,I2
!       C
!       C     CONDITION FOR MISSING VALUES OF THE
!       C     FILTER AT THE END OF THE PROFILE
!       C
!             IF(J .GT. NF) GO TO 30
!             SUME=SUME+FC(N)*ES(J)
!             SUMF=SUMF+FC(N)
!             N=N+1
!       30    CONTINUE
!             ES(I)=SUME/SUMF
!       20    CONTINUE
!             RETURN
```